AGU PUBLICATIONS

Global Biogeochemical Cycles

RESEARCH ARTICLE
10.1002/2014GB004903

Key Points:
- Surface biogeochemical cycle of cobalt assessed in the western Atlantic Ocean
- Recycling sustain the biological requirement for cobalt in subtropical domains
- The atmospheric and Amazon inputs affect the cobalt distribution

Supporting Information:
- Readme
- Table S1
- Figure S1
- Figure S2
- Text S1

Correspondence to:
G. Dulaquais,
gabriel.dulaquais@univ-brest.fr

Citation:
Dulaquais, G., M. Boye, R. Middag, S. Owens, V. Puigcorbe, K. Buesseler, P. Masqué, H. J. W. de Baar, and X. Carton (2014), Contrasting biogeochemical cycles of cobalt in the surface western Atlantic Ocean, *Global Biogeochem. Cycles*, *28*, 1387–1412, doi:10.1002/2014GB004903.

Received 24 MAY 2014
Accepted 26 OCT 2014
Accepted article online 29 OCT 2014
Published online 5 DEC 2014

Contrasting biogeochemical cycles of cobalt in the surface western Atlantic Ocean

Gabriel Dulaquais[1], Marie Boye[1], Rob Middag[2,3], Stephanis Owens[4], Viena Puigcorbe[5], Ken Buesseler[4], Pere Masqué[5,6,7], Hein J. W. de Baar[2], and Xavier Carton[8]

[1]Laboratoire des Sciences de l'Environnement Marin UMR6539, Institut Universitaire Européen de la Mer, Technopôle Brest Iroise, Plouzané, France, [2]Department of Marine Chemistry and Geology, Royal Netherlands Institute for Sea Research, Den Burg, Netherlands, [3]Department of Chemistry, University of Otago, Dunedin, New Zealand, [4]Woods Hole Oceanographic Institution, Woods Hole, Massachusetts, USA, [5]Institut de Ciencia i Tecnologia Ambientals and Department of Physics, Univertsitat Atonoma de Barcelona, Bellaterra, Spain, [6]Oceans Institute and School of Physics, University of Western Australia, Crawley, Western Australia, Australia, [7]School of Natural Sciences and Centre for Marine Ecosystems Research, Edith Cowan University, Joondalup, Western Australia, Australia, [8]Laboratoire de Physique des Océans, Université de Bretagne Occidentale-UFR Sciences, Brest, France

Abstract Dissolved cobalt (DCo; <0.2 μm; 14 to 93 pM) and the apparent particulate cobalt (PCo; >0.2 μm; <1 to 15 pM) were determined in the upper water column (<1000 m) of the western Atlantic Ocean along the GEOTRACES-A02 section (64°N to 50°S). The lowest DCo concentrations, typical of a nutrient-type distribution were observed in surface waters of the subtropical domains. Strong linear relationships between DCo and phosphate (P) as well as meridional gradients of decreasing DCo from high latitudes were characterized and both linked to the Co biological requirement. External sources such as the Amazon and the atmospheric deposition were found to contribute significantly (>10%) to the DCo stock of the mixed layer in the equatorial and north subtropical domains. Biotic and abiotic processes as well as the physical terms involved in the biogeochemical cycle of Co were defined and estimated. This allowed establishing the first global budget of DCo for the upper 100 m in the western Atlantic. The biological DCo uptake flux was the dominant sink along the section, as reflected by the overall nutrient-type behavior of DCo. The regeneration varied widely within the different biogeochemical domains, accounting for 10% of the DCo-uptake rate in the subarctic gyre and for up to 85% in southern subtropical domain. These findings demonstrated that the regeneration is likely the prevailing source of DCo in the surface waters of the western Atlantic, except in the subpolar domains where physically driven sources can sustain the DCo biological requirement.

1. Introduction

Cobalt (Co) is an essential trace nutrient required as the central atom of vitamin B_{12} (cobalamin) [*Bertrand et al.*, 2007]. Cobalt can also substitute for zinc involved as a cofactor in the carbonic anhydrase and the alkaline phosphatase that are essential for the acquisition of inorganic carbon and dissolved organic phosphorus by phytoplankton, respectively [*Lane and Morel*, 2000; *Gong et al.*, 2005]. Cobalamin is also used by bacteria and archaea for anaerobic processes such as fermentation or dehalogenation [*Swanner et al.*, 2014, and reference therein]. Moreover, cyanobacteria like *Prochlorochoccus* sp., which often dominate the picophytoplankton assemblage and account for a significant proportion of the primary production in oligotrophic regions, have an absolute requirement for Co [*Campbell et al.*, 1994; *Sunda and Huntsman*, 1995; *Saito et al.*, 2002]. The elemental compositions of phytoplankton also suggest that Co is an important micronutrient for the coccolithophorids, diatoms, and dinoflagellates [*Ho et al.*, 2003].

Previous studies have reported a nutrient-type distribution of dissolved cobalt (DCo) in surface waters of oligotrophic and temperate domains [*Martin et al.*, 1993; *Saito and Moffett*, 2002; *Jakuba et al.*, 2008; *Noble et al.*, 2008], which is related to its biological uptake by cyanobacteria [*Saito et al.*, 2002; *Saito and Moffett*, 2002; *Bown et al.*, 2011]. Other surface distribution patterns have been observed, notably a nearly conservative-type behavior in the Southern Ocean associated with a low biological uptake of DCo by the Antarctic diatoms [*Bown et al.*, 2011].

Previous field studies have reports a correlation between DCo and the macronutrient phosphate (P) in surface waters of different biogeochemical domains, indicative of their proportional biological uptake [*Saito et al.*, 2004;

Noble et al., 2008; *Saito et al*., 2010; *Bown et al*., 2011]. Those studies also showed that the DCo/P depletion ratio varied between the oceanic domains, potentially reflecting differences in the phytoplankton assemblage and productivity, as well as regional variations in the input of DCo (and/or P). Thus, this comprehensive survey of DCo distributions across oceanic provinces will also increase our understanding of the coupling between DCo and P in the surface waters.

Previous estimates suggested that biological uptake is the prevailing sink of DCo in oligotrophic waters [*Saito et al*., 2002; *Bown et al*., 2011]. Indeed, biological uptake can be significantly higher than other removal mechanisms of DCo from surface waters such as cooxidation with manganese through microbial oxidation [*Moffett and Ho*, 1996; *Saito et al*., 2004] or export by adsorption (scavenging) on settling particles [*Bown et al*., 2011]. An indirect estimate suggested that recycling of Co in surface waters due to abiotic processes, microbial loop, cell lysis, and grazing, could sustain up to 70–90% of the DCo biological uptake in the subtropics of the southeastern Atlantic [*Bown et al*., 2011]. However, the terms that drive the internal cycle of DCo in the upper ocean need to be better assessed, notably the regeneration flux of DCo in surface waters, considering its potential importance in the Co cycle.

Among the external sources, the deposition of dust from the Patagonian and the Sahara deserts has been shown to be an important source of Co in the surface waters of the southwestern Atlantic and the central northern Atlantic, respectively [*Gaiero et al*., 2003; *Baker et al*., 2007]. For example, the relative DCo maximum observed in subsurface waters of the Sargasso Sea has been related to significant atmospheric Co input during the late summer [*Shelley et al*., 2012]. In other regions, the atmospheric deposition is likely negligible, such as the southeastern Atlantic [*Bown et al*., 2011] and southcentral Atlantic [*Noble et al*., 2012]. However, there are still large uncertainties in estimates of the atmospheric deposition of Co in the surface waters, due to the limited data on the fractional solubility of Co in aerosols and on the elemental compositions of the dust that vary depending on their provenance. By taking into account some of this spatial variability, our study reassesses the atmospheric deposition of Co in the western Atlantic.

The observation of an inverse linear relationship between DCo and salinity in the northwestern Atlantic [*Saito and Moffett*, 2002] and the western equatorial Atlantic [*Tovar-Sanchez and Sañudo-Wilhelmy*, 2011] suggest that freshwater may be another external source of DCo in the surface western Atlantic. For instance, the Amazon River represents a significant source of many elements to the western equatorial Atlantic [*Boyle et al*., 1982]; however, its importance to DCo needs to be better constrained. Recent work has also hinted at the importance of lateral advection of water masses enriched in DCo following contact with continental margins in the southeastern Atlantic [*Bown et al*., 2011] and of the diffusion from intermediate waters in the frontal areas of the western Atlantic [*Dulaquais et al*., 2014]. With only a first, tentative budget made for the southeastern Atlantic and the Southern Ocean [*Bown et al*., 2011], the sources and biogeochemical cycle of Co are still poorly constrained in the surface waters.

Despite these major advances, the oceanic behavior of DCo in the surface waters is still not well understood, with little data on DCo distribution in the global ocean. In this respect, a survey along a large radial in the entire western Atlantic Ocean was consider to be an ideal scheme to observe the changes in the surface vertical distribution of DCo across contrasting biogeochemical domains. In this study we investigate the meridional distributions of DCo and the apparent particulate cobalt (PCo) in the upper 1000 m along a section in the western Atlantic Ocean. Spanning from the East coast of Greenland (64°N) to the Malvinas Plateau (50°S) the radial encountered several biogeochemical domains. Two oligotrophic subtropical areas, the equatorial zone, and the subpolar and subantarctic latitudes in the extremities of the section were crossed. The distribution of Co is discussed in the context of the biogeochemical and physical features of the domains and the external inputs from the atmosphere and the Amazon in order to determine the various sources and sinks of Co. The coupling of Co with the macronutrient P and the potentially significant role of Co regeneration in surface waters of the western Atlantic are also discussed. By parameterizing the different processes involved in the Co cycle, a tentative budget for Co in the upper 100 m is presented on the scale of the individual domains and the western Atlantic basin.

2. Method

2.1. Cruise Track and Sampling

Seawater samples were collected during four cruises along the GEOTRACES-A02 section spreading from 64°N to 50°S in the western Atlantic Ocean that were conducted between 2010 and 2012 (Figure 1). A total

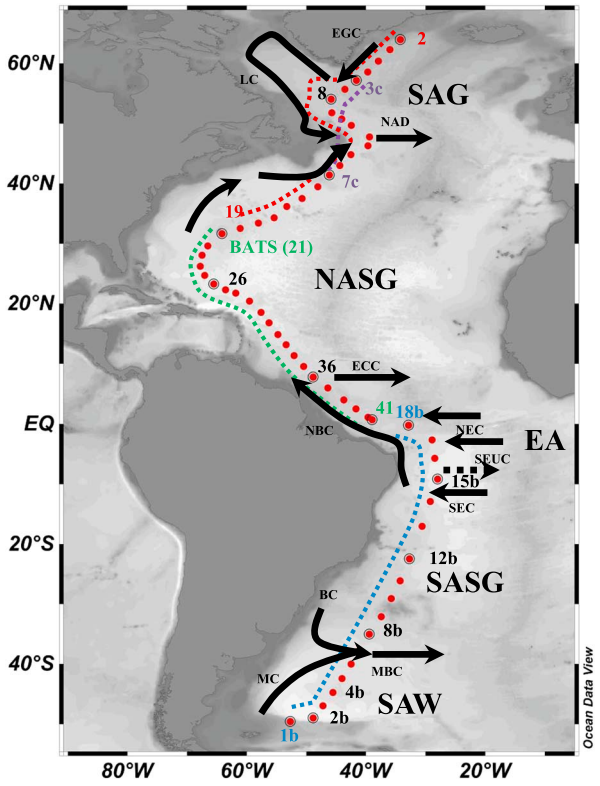

Figure 1. (a) Surface physical features and cruise track along the GEOTRACES-A02 section. (b) Sampling location of the different four Legs are shown (Leg 1 in red dashed line from station 2 to station 19, Leg 2 in green dashed line from station 21 to station 41, Leg 3 in blue dashed line from station 1b to 18b, and Leg 4 in purple dashed line from station 3c to 7c).

of 47 stations with a vertical resolution of 6–10 depths between 9 m and 1000 m were sampled for dissolved cobalt analyses (DCo), and 15 stations for total (unfiltered) cobalt determinations (TCo). The apparent particulate cobalt concentrations (PCo) were calculated by subtraction of DCo from TCo. The complete data set of cobalt (dissolved, total, and apparent particulate) at all stations is available at the international GEOTRACES data center (http://www.bodc.ac.uk/geotraces/).

Samples were collected using the TITAN-CTD frame [*de Baar et al*., 2008] of Nederlands Instituut voor Onderzoek der Zee (Netherlands), with 24 ultraclean sampling bottles of 24.4 L each made of (polyvinylidene fluoride) PVDF plastic [*Rijkenberg et al*., 2014]. The frame was placed in a Class-100 container for subsampling [*de Baar et al*., 2008]. Unfiltered samples were transferred into acid cleaned 250 ml Nalgene® Low-Density Polyethylene (LDPE) bottles for TCo analyses. The samples for DCo analyses were collected after filtration using 0.2 µm Sartobran® 300 (Sartorius) cartridges under pure N_2 pressure (filtered 99.99% N_2, 0.7 atm) in acid cleaned 250 ml or 500 ml Nalgene® LDPE bottles. All samples were acidified using ultrapure HCl® (Merck, 0.01 M) immediately after their collection. Then the acidified samples were stored in double bags in the dark and at ambient temperature, before later analyses in the shore-based laboratory.

2.2. Analytical Method for Cobalt Analyses

2.2.1. Method

Prior to the analyses, the samples were UV digested [*Saito and Moffett*, 2002; *Shelley et al*., 2010] for 3 h in acid clean silica tubes using a 600 W high-pressure mercury vapor lamp [*Bown et al*., 2011; *Dulaquais et al*., 2014], and left for an equilibration time of 48 h. Dissolved and total cobalt concentrations were determined by Flow-Injection Analysis (FIA) and chemiluminescence detection following the method adapted from *Shelley et al*. [2010], as described in *Bown et al*. [2011] and *Dulaquais et al*. [2014]. The system consists of one 10-ports injection valve (VICI valves from VALCO instruments) which operates as an autosampler, and of two microelectronically actuated injection valves (VICI valves from VALCO instruments) to inject the sample and the reagents using Tygon® tubes. The flow injection is provided by a peristaltic pump (205 CA, Watson Marlow).

The reagents are prepared with trace metals quality reagents under a laminar flow hood (ADS Laminaire, International Organization for Standardization 5 class) with ultrapure water (MiliQ, 18.2 mΩ) the day before the analysis and kept at room temperature for an overnight equilibration [*Dulaquais et al*., 2014].

The sample were buffered online with ammonium acetate (0.3 M, American Chemical Society (ACS) Reagents), and loaded on an IDA-Toyopearl chelating resin to preconcentrate the cobalt contained in each sample. Then a HCl solution (0.1 M, Suprapur® Merck) was injected through the column to elute Co. The eluate was warmed in a 60°C thermostatic bath. The detection system consists of a photomultiplier detector (Hamamatsu, H9319 Series). The injection valves and the photomultiplier detector are operated on a laptop computer by

Table 1. Comparison of Dissolved Cobalt Analyses Obtained in the UV-Oxidized Samples by the FIA-Chemiluminescence Method Used in the Present Study With Consensus Values Reported by the Sampling and Analysis of Iron (SAFe) and GEOTRACES Programs

Sample	DCo Measured (pM)	Consensus Value (pM)
SAFe S	5.1 ± 2.2 (n = 25)	4.8 ± 1.2
SAFe D1	42.3 ± 1.4 (n = 15)	45.4 ± 4.7
SAFe D2	44.2 ± 1.7 (n = 25)	45.7 ± 2.9
GEOTRACES S	29.8 ± 2.0 (n = 35)	31.8 ± 1.1
GEOTRACES D	63.2 ± 2.3 (n = 25)	65.2 ± 1.2

amodified Labview® 8.4 interface (E. Duvieilbourg and M. Boye, Laboratoire des Sciences de l'Environnement Marin (LEMAR). The electrical devices are connected to a modulator of current (ELLIPSEMAX 600, MGE/UPS Systems).

The Co concentrations were calibrated against two calibration lines made with standard additions of cobalt of 0, 12.5, 25, 50, 75, and 100 pM to seawater, and performed before and after each series of 8 or 12 samples. TCo and DCo concentrations are based on triplicate analyses of each sample using the mean peak height of the chemiluminescent signal, and they are corrected with respect to blank analyses. Two to four reagent blanks including the buffer blank were analyzed per series of 8–12 samples at the beginning and at the end of the series, in acidified MilliQ water instead of the sample [*Bowie and Lohan*, 2009; *Bown et al*., 2011].

The final standard deviation of the measurement is calculated by propagating the uncertainties on blanks, the calibration curves and the deviation of the triplicate analyses. A t test was applied to verify that the difference between TCo and DCo is significant to allow reliable estimation of PCo concentration. The standard error on PCo is calculated by combining uncertainties of DCo and TCo measurements ($SD_{PCo} = (SD_{DCo}^2 + SD_{TCo}^2)^{0.5}$).

2.2.2. Analytical Performance

The mean reagent blank (based on all blank determinations) was 4.2 ± 2.1 pM of Co in MilliQ (n =180). The limit of detection of the method estimated as three times the standard deviation of the mean reagent blank was thus 6.3 pM of Co (n = 180). Each series of samples was validated by running samples previously collected during the Sampling and Analysis of Iron (SAFe) program or the GEOTRACES program, following the same procedure as describe above. The DCo concentrations we measured in the SAFe and GEOTRACES reference samples were in excellent agreement with the consensus values (Table 1, www.geotraces.org). The analytical precision of the method was determined from repeated analyses of the surface GEOTRACES (GS) reference sample, yielding an uncertainty of ±3.8% expressed as relative standard deviation on the mean (n = 15). Despite our agreement with the consensus values, some new concerns have recently emerged regarding possible losses of DCo due to storage protocol. Some underestimation of DCo could indeed result from storage of nonacidified samples collected in low O_2 and/or high-dust environments; this effect should be minor for samples from the South Atlantic and similar regions, but may be more pronounced for North Atlantic samples due to the very high dust loads (M. Saito, WHOI, personal communication, 2014). Additional work should be done to further assess this potential storage artifact, especially when the samples are acidified before storage as we have done for our samples and the GEOTRACES and SAFE reference samples.

2.3. Hydrography

Hydrological parameters (salinity (S), temperature (T), dissolved oxygen (O_2), conductivity, fluorescence, and turbidity) were measured using a SBE9 + underwater sensor, a SBE3 + thermometer (±0.001°C), a SBE4 conductivity sensor (±0.3 mS s^{-1}), a SBE43 dissolved oxygen sensor (±2%), a Chelsea Aquatracka MKIII fluorometer (±0.2 µg L^{-1}), and a Wetlabs C-Star transmissiometer (±0.02% °C^{-1}).

2.4. Macronutrients Analysis

Seawater samples for nutrient analysis were collected the ultraclean sampling bottles (PVDF) describe above and transferred to 125 ml polypropylene bottles. All the nutrients were analyzed onboard by colorimetric methods following the methods of *Murphy and Riley* [1962] for phosphate (PO_4^{3-}), *Strickland and Parsons* [1968] for silicate ($Si(OH)_4^-$), and *Grasshoff et al*. [1983] for nitrate (NO_3^-) and nitrite (NO_2^-). The detection limits of the methods (3σ after 24 analyses of the same sample) were 18 nM for phosphate, 252 nM for silicate, 190 nM for nitrate, and 3 nM for nitrite [*van Ooijen*, 2010].

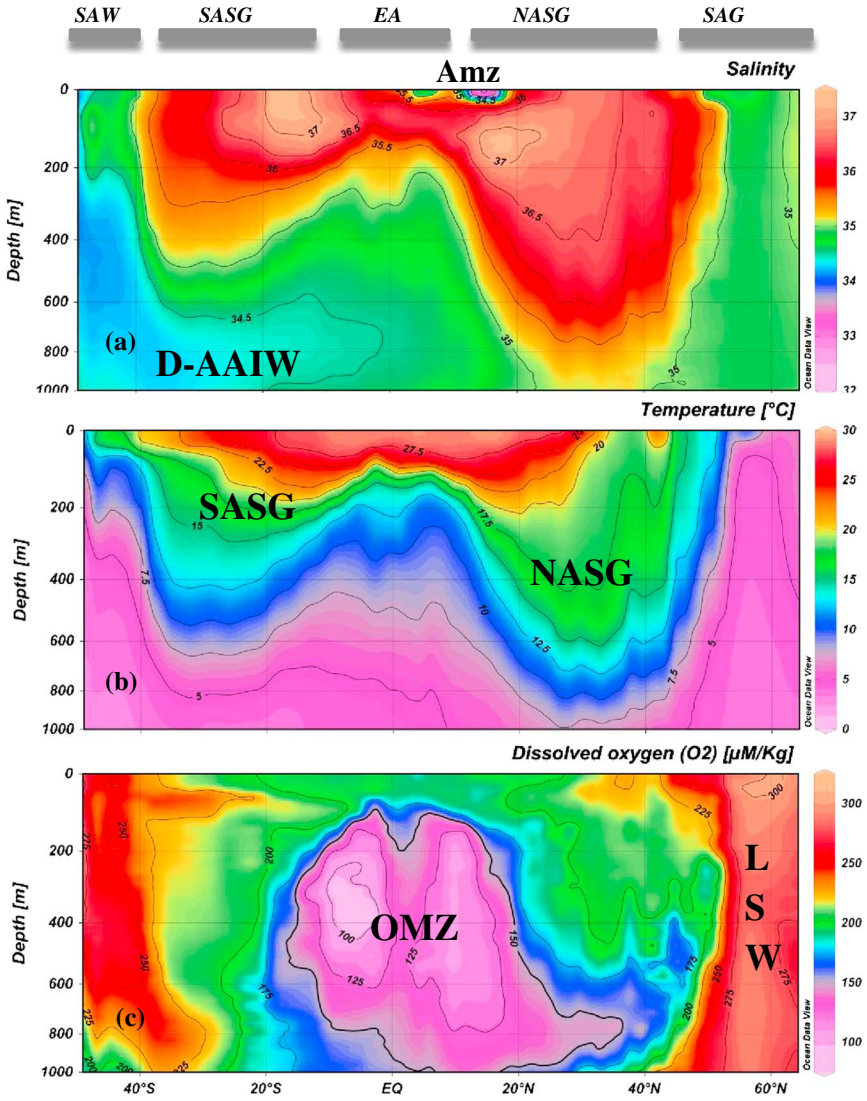

Figure 2. Interpolated vertical sections in the upper 1000 m of (a) temperature (TMP), (b) salinity (*S*), and (c) dissolved oxygen along the GA02 section, based on CTD data. Drake Antarctic Intermediate Waters (D-AAIW), Amazon River influence (Amz), South Atlantic Subtropical Gyre (SASG), North Atlantic Subtropical Gyre (NASG), Labrador Sea Waters (LSW) and Oxygen Minimum Zone (OMZ) are indicated.

3. Results

3.1. Dynamical Features

The different surface physical features along the section are presented on Figure 1. In the North, the section crossed the subarctic Gyre (SAG) between 64°N and 50°N, where the Labrabor Sea Water (LSW) dives to form, with the Arctic Bottom Water, the Western North Atlantic Deep Water. In this area, the surface currents (East Greenland Current and Labrador Current induce a mean southward flow. The well oxygenated and dense waters of the subarctic gyre are separated, in the south, by the North Subtropical Front (NSTF) at ~45°N from the relatively low-oxygenated, saline, and warm waters of the North Atlantic Subtropical Gyre (NASG). The NSTF is characterized by high-temperature anomaly (+5°C) and by a strong eastward geostrophic current in surface waters (data not shown), likely the North Atlantic Drift [*Reid*, 1994], known for its important role on climate regulation [*Minobe et al.*, 2010].

In the NASG, low-density waters occur in the top 600 m due to relatively high salinity and temperature ($S > 35$, $T > 10$°C; Figure 2). However, at 15°N and to a lesser extent at 4°N these saline waters were covered

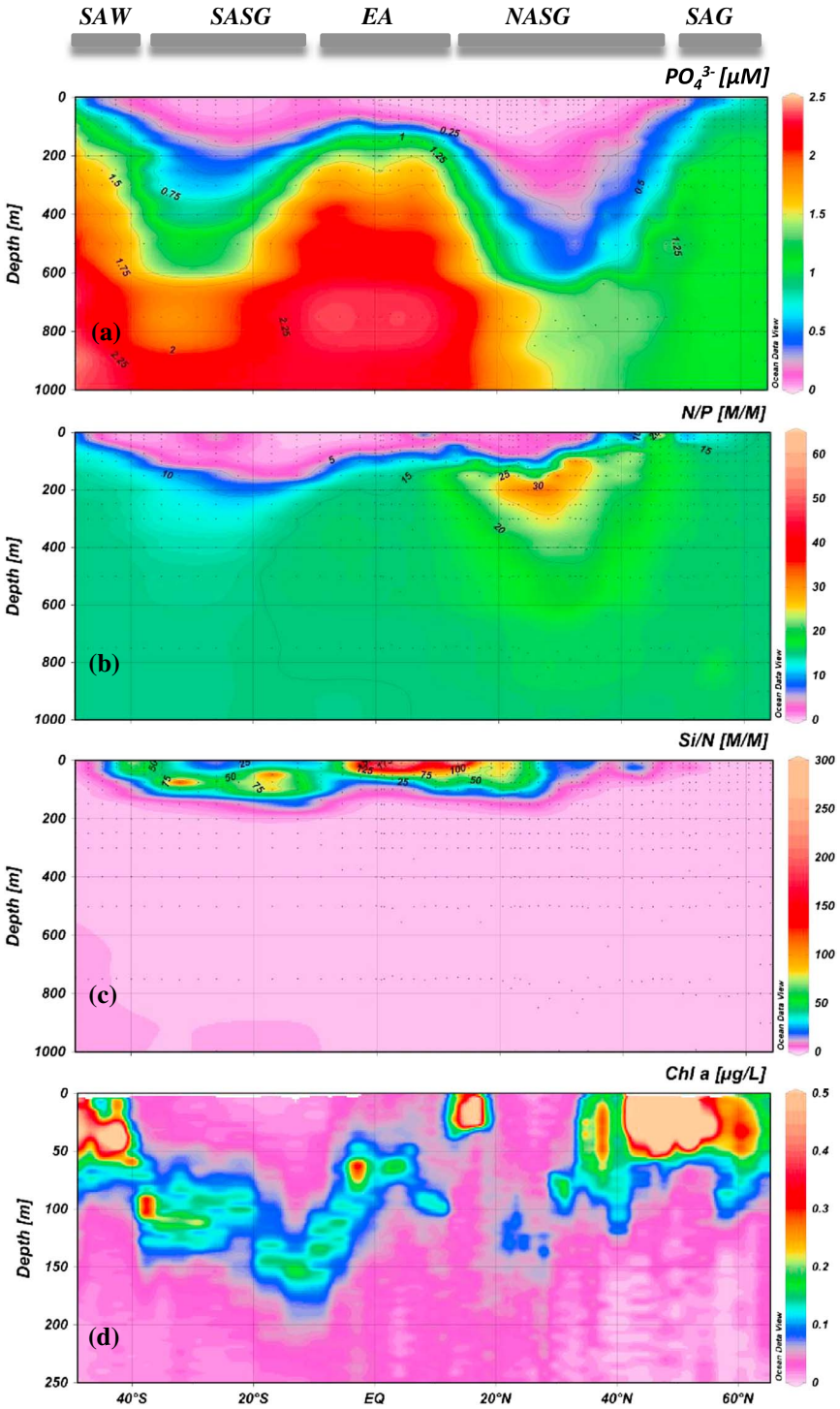

Figure 3. Interpolated vertical sections in the upper 1000 m of (a) phosphate, (b) N:P ratio, (c) Si/N ratio, based on 735 analyses of water column samples collected along the GA02 section, and (d) Chl *a* distribution in the upper 250 m derived from CTD data.

by relatively fresh waters (Figure 2, $32.1 < S < 34.9$), originating from the Amazon plume. The waters influenced by the Amazon plume were also characterized by high Si:N ratio (Figure 3c).

Leaving the NASG southward, the section enters the equatorial area. Here the zonal geostrophic velocities (not shown) indicate the presence of several surface and subsurface jets (Figure 1). The North Equatorial

Current (NEC, at 5–10°N), the North Equatorial Countercurrent (NECC, at ~3°N; 0.2 m s^{-1}), the South Equatorial Current (SEC, at 5–10°S) and the South Equatorial Undercurrent (SEUC, at ~5°S, 0.12 m s^{-1} 200 m depth) [*Peterson and Stramma*, 1991; *Stramma and England*, 1999] can thus be located. The equatorial domain is bordered by the NEC in the North and by the SEC in the South, both of which were characterized by westward surface geostrophic propagating vectors and similar speed (respectively, 0.15 and 0.2 m s^{-1}). A mean flow toward the northwest, the north Brazil current (NBC), results from these equatorial surface currents. This equatorial current system supplies eddies to the northern subtropical domain [*Oschlies and Garçon*, 1998]. Additionally, under these surface currents, an oxygen minimum zone (OMZ; $O_2 < 150$ μM) was also observed between 150 and 600 m (Figure 2c). Part of this low O_2 signature was due to the advection of the poorly oxygenated Atlantic Central Waters ($O_2 < 50$ μM) [*Noble et al*., [2012], flowing westward from the African shelf across the Atlantic basin.

Southward the section enters into the South Atlantic Subtropical Gyre (SASG). South of the SASG, in addition to strong eddy activity in this area as observed in the geostrophic current field, the Malvinas-Brazil confluence (MBC), an eastward jet resulting from the Brazil current (BC) flowing southward and the Malvinas Current (MC) flowing northward, can be located in the Argentine basin at around 40°S (e.g., at station 6b; geostrophic data not shown). The saline and relatively oxygen-poor waters of the MBC separate the SASG from the subantarctic Waters (SAW). At depth the Drake Antarctic intermediate waters (D-AAIW) are flowing northward in the southern part of the section.

3.2. Biogeochemical Provinces

The different biogeochemical domains characterized along the section (Figure 3) were mostly delineated by the frontal and jet systems described above (Figure 1). The surface waters of the SAG were marked by relatively high-phosphate and nitrate concentrations ($NO_3^- > 10$ μM, data not shown; $PO_4^{3-} > 0.8$ μM). Furthermore, the Chlorophyll *a* levels observed in the southern side of the SAG and lower nutrients concentrations (e.g., Chl $a = 1.9$ μg L^{-1}, $NO_3^- < 1$ μM, $PO_4^{3-} < 0.2$ μM at station 10–49°N, 24 m depth, Figure 3) suggested the occurrence of a phytoplankton bloom. In the upper 100 m of the two subtropical domains the extremely low nutrients concentrations (such as observed in the NASG: $PO_4^{3-} < 0.5$ μM; $NO_3^- < 5$ μM, Si < 5 μM) and the subsurface Chlorophyll *a* values (Chl $a_. < 0.03$ μg/L, Figure 3d) were characteristic of oligotrophic conditions. In these domains, the N/P ratios were generally below the Redfield ratio in the upper 100 m waters (Figure 3b) suggesting that nitrogen might be more limiting than phosphorus. However, a greater depletion of nitrogen relative to phosphate was observed in the upper 300 m of the SASG (N:P < 10) compared to the NASG (N:P > 25; Figure 3b) [*Dulaquais et al*., 2014] likely due to a greater proportion of N_2 fixers, such as diazotrophic cyanobacteria, in the NASG than in the SASG [*Mather et al*., 2008]. In the equatorial area, low-nutrients concentrations were observed in the upper 100 m ($NO_3^- < 0.8$ μM; $PO_4^{3-} < 0.1$ μM; Si < 1.3 μM), whereas high concentrations of nitrate and phosphate ($NO_3^- > 34$ μM; $PO_4^{3-} > 2.3$ μM) and low levels of silicate (5 μM < Si < 15 μM) were recorded at intermediate depths due to the incursion of the Atlantic Central Waters [*Dulaquais et al*., 2014]. In this area, the Chl *a* levels were similar to those recorded in the oligotrophic domains. South of the MBC, the influence of the AAIW and upper circumpolar deep waters (UCDW) generated a southward gradient of nutrients in the top 1000 m layer (Figure 3a) with increasing concentrations southward. Relatively high-nutrient concentrations were generally observed in the top 200 m depths ($NO_3^- > 20$ μM; $PO_4^{3-} > 1.2$ μM; Si > 15 μM). In the southern latitudes of the section, the Chl *a* concentrations >0.5 μg L^{-1} and the high levels of nitrite ($NO_2^- > 0.16$ μM) observed in the upper 100 m layer, associated with the depletion of silicate levels (Si < 1.2 μM) and the low Si:N ratio (<0.2) (Figure 3c), hinted at the final stages of a diatom bloom.

3.3. The Distributions of Cobalt in Surface Waters of the Western Atlantic

The meridional and vertical distributions of DCo and PCo are presented in the upper 1000 m along the section in Figure 4. Dissolved cobalt concentrations ranged from 14.7 ± 1.4 to 93.3 ± 3.3 pM along the section and mostly follow a nutrient-like behavior in the upper 1000 m (Figure 4a). The lowest concentration was observed in surface waters of the SASG (e.g., at 9 m depth at station 11b-26°S), whereas the highest were recorded in the OMZ of the equatorial area (e.g., at station 15b-9°S at 290 m depth). The vertical distributions of PCo generally exhibited higher concentrations in the subsurface and decreasing concentrations with depth (Figure 4b). PCo concentrations ranged from near undetectable values to 15.2 ± 2.3 pM (e.g., at station

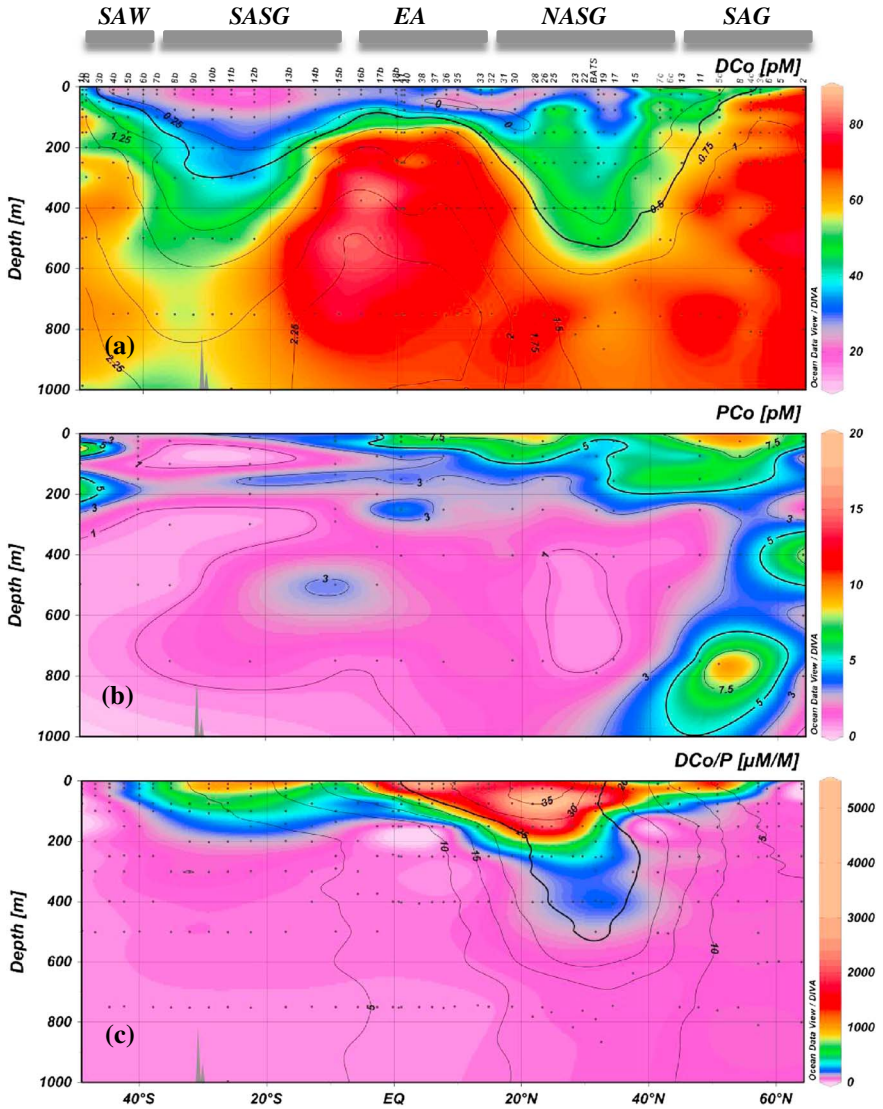

Figure 4. Interpolated vertical section in the upper 1000 m of (a) dissolved cobalt concentration (DCo) with phosphate contours overlaid on the profile, (b) particulate cobalt concentrations (PCo), and (c) DCo/P ratio with dissolved aluminium concentration (DAl) contours overlaid on the profile (Middag et al., unpublished data).

5c-50.8°N at 761 m depth). The relative proportion of PCo to TCo (Figure 5a) ranged from less than 5% at several stations in the intermediate waters (250–1000 m) to up to 34% (at station 26–25 m depth), with a mean of 12 ± 12% ($n = 76$), indicating that cobalt was primarily present in the dissolved fraction. Furthermore, the relative proportion of PCo covaried with the Chl *a* distribution (Figures 5a and 5b).

Distinct vertical distributions of DCo were observed in the surface waters of the different biogeochemical domains (Figures 6). At the highest latitudes of the northern subarctic gyre, high DCo concentrations were measured (about 60–70 pM; Figures 4a and 6a). Here the particulate cobalt was howed similar in terms of concentration and vertical distribution to those observed by *Weinstein and Moran* [2004], with relative PCo maxima in the subsurface (ranging from 5.9 ± 1.0 to 10.4 ± 2.0 pM), and decreasing concentrations with depth (Figure 6f). In the southern side of the SAG, high PCo concentrations were observed in the Chl *a* maximum (at station 11; 25 m PCo = 8.2 pM). Lower DCo concentrations were detected in surface waters of this region (Figure 6a) in August 2012 during Leg-4 (e.g., mean $DCo_{25m} = 43.2.$ ±1.6 pM $n = 2$) compared to measurements in samples collected in April 2010 during Leg-1 (e.g., mean $DCo_{25m} = 64.6 \pm 5.4$ pM at 25 m $n = 4$).

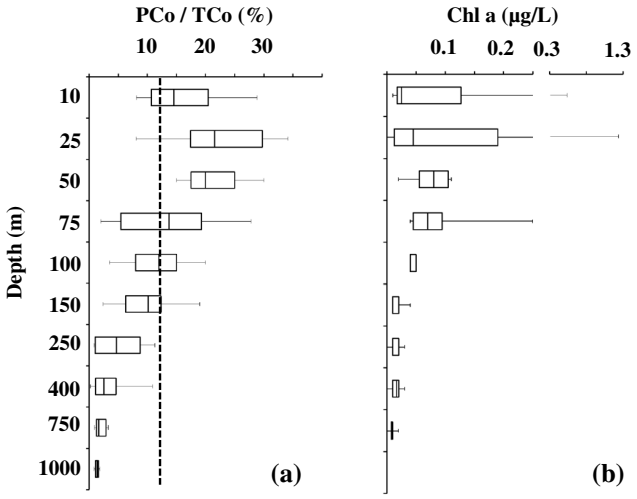

Figure 5. (a) Box plot representing the relative proportion of particulate cobalt (PCo) to total cobalt (TCo) using all data for a given depth along the section. Dashed line represents the average (mean = 12 ± 12%; $n = 76$). (b) Box plot representing estimated Chl *a* (derived from CTD data) using all data, where PCo is available, for a given depth along the section.

DCo was depleted in the surface waters of both subtropical domains and its concentration increased with depth below the nutricline, featuring a nutrient-like distribution (Figures 4a, 6b, and 6d). The concentrations of DCo were slightly lower in the SASG (mean $DCo_{\int 100m} = 24 \pm 5$ pM) compared to those recorded in the NASG (mean $DCo_{\int 100m} = 33 \pm 8$ pM). Furthermore, the PCo distribution also showed, like DCo, lower concentrations in the subsurface waters of the SASG (<5 pM; Figure 6i) compared to the NASG (>5 pM; Figure 6 g). Additionally, relative maxima of DCo were observed at about 10 m depth at a few stations in the NASG (as exemplified for station 26, Figure 6b).

In the equatorial area, the DCo distribution was characterized by low concentrations in the top 100 m (mean $DCo_{\int 100m} = 30 \pm 9$ pM, $n = 44$) and a

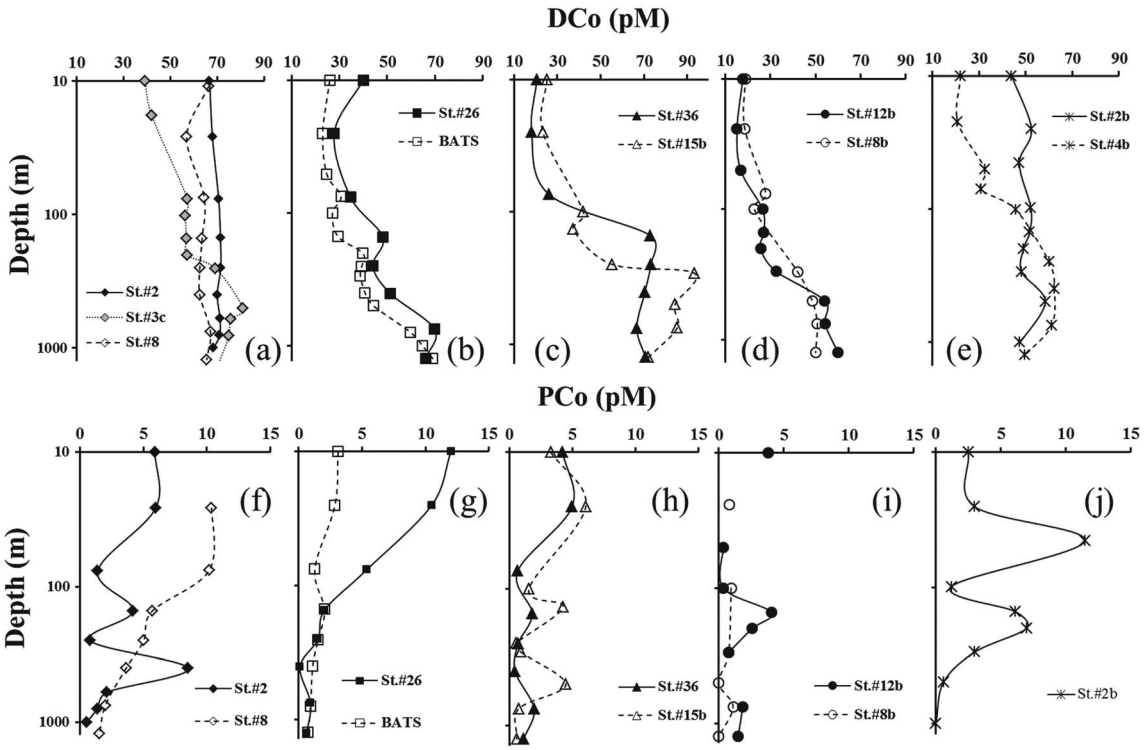

Figure 6. Typical vertical distribution of dissolved (DCo) and particulate (PCo) cobalt against depth in the different biogeochemical domains. In the SAG, (a) DCo and (f) PCo are shown for station 2 (Leg-1; 64°N 34.25°W), station 8 (Leg-1; 54°N 45.84°W), and station 3c (Leg-4; 57°N 44°W). In the northern subtropical domain, (b) DCo and (g) PCo are shown at station 26 (Leg-2; 23°N 65.55°W) and at the BATS station (Leg-2; 31.7°N 64.2°W). In the equatorial area, (c) DCo and (h) PCo are presented at station 36 (Leg-2; 7.8°N 48.9°W) and station 15b (Leg-3; 9°S 28°W);). In the southern subtropical domain, (d) DCo and (i) PCo are shown for station 12b (Leg-3; 22.47°S 32.7°W) and station 8b (Leg-3; 35°S 39.4°W). In the subantarctic area (e) DCo and (j) PCo are shown at station 12b (Leg-3; 49°S 48.9°W) and station 4b (Leg-3; 44.7°S 45.6°W).

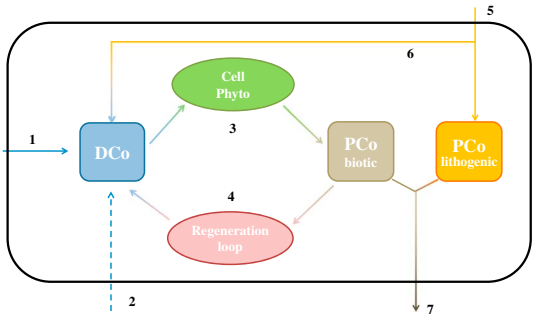

Figure 7. Simplistic conceptual schema of the cobalt cycling in the upper 100 m. Arrows represent the fluxes as follows: 1: lateral advection; 2: vertical diffusion; 3: uptake; 4: regeneration; 5: Co deposition; 6: dust dissolution; and 7: export. Here scavenging could not be discerned from biological uptake and is considered negligible.

sharp increase between 100 and 250 m (mean $DCo_{[100–250m}$ = 62 ± 13 pM, n = 10), that continued to increase to reach maximum values at about 400 m depth (mean $DCo_{[250–400m}$ = 73 ± 10 pM, n = 19) (Figures 4 and 6c). These maximum concentrations were the highest values recorded along the section, reaching values up to 93.3 ± 3.3 pM (at 9°S), and strongly correlated with the oxygen depletion ($\Delta DCo/\Delta O_2 = -0.28$ μM/M, $R^2 > 0.66$) as reported by *Dulaquais et al.* [2014]. The distribution of PCo in this equatorial domain was similar to that observed in the other domains, with relatively high concentrations in surface waters (PCo > 5 pM, Figure 6 h), reaching a maximum value of 10.2 ± 2.1 pM observed at 10 m at station 40 (1.15°N).

South of the Brazil-Malvinas confluence, in the subantarctic waters, a surface southward increasing gradient of DCo was observed (Figure 4a), and the vertical distribution of DCo showed nutrient distribution in the upper 200 m, below which the concentrations were relatively constant. At these latitudes, the highest DCo concentrations were recorded in the core of D-AAIW (100–600 m; Figure 6e).

4. Discussion

With the aim to better constraining the biogeochemical cycle of cobalt in the surface western Atlantic, regional variability in the DCo:P relationship is discussed and key fluxes, conceptualized in Figure 7, are estimated. We propose an estimate of the regeneration rate of DCo in surface waters due to a combination of abiotic processes, the microbial loop, cell lysis, and grazing. We also evaluate the external inputs of Co from the atmosphere and the Amazon River to the surface western Atlantic. Surface (100 m) Co budgets are proposed the different biogeochemical domains of the western Atlantic.

4.1. Internal Cycle of Dissolved Cobalt in the Surface Western Atlantic

4.1.1. The Dissolved Cobalt and Phosphate Relationship

The vertical distribution of DCo was nutrient-like, akin to the macronutrient phosphate (P) in the oligotrophic and tropical surface waters (Figure 4a). Strong linear correlations between DCo and P have been previously reported in the surface waters of subtropical regions in the South Pacific [*Ellwood*, 2008], the northeast Pacific [*Sunda and Huntsman*, 1995], the North Atlantic [*Martin et al.*, 1993], and the Sargasso Sea [*Saito and Moffett*, 2002; *Jakuba et al.*, 2008], as well as in other oligotrophic systems [*Saito and Moffett*, 2002; *Bown et al.*, 2011], or in upwelling [*Saito et al.*, 2004], in eddies near islands [*Noble et al.*, 2008], and in Antarctic waters of the Ross Sea [*Saito et al.*, 2010]. These correlations suggested that the biological uptake of DCo is proportional to that of P in the surface waters [*Jakuba et al.*, 2008; *Noble et al.*, 2008; *Bown et al.*, 2011]. Along the section sampled here, when all the data are considered, a linear relationship between DCo and P concentrations was also obtained in the surface layer (0–250 m) providing a mean DCo:P slope of 23.1 μM M^{-1} ($R^2 > 0.53$, n = 231; Figure 8a). However, the slopes of DCo:P correlations varied across the different biogeochemical domains crossed along the section (Figure 8b), with the highest DCo:P slopes observed in the two subtropical domains (>50 μM M^{-1}). These regional differences in DCo:P could reflect differences in phytoplankton assemblages between the domains, since a wide range of internal Co:P cellular quota have been reported for different phytoplankton species [*Ho et al.*, 2003; *Cullen et al.*, 2003; *Tovar-Sanchez et al.*, 2006; *Twining et al.*, 2011; *Twining and Baines*, 2013]. Other factors could account for the regional differences in DCo:P ratios, including differences in the surface regeneration rate, external sources, and/or physical processes [*Noble et al.*, 2008].

A mean DCo:P slope of 31.2 μM M^{-1} (R^2 = 0.78; n = 28) was found in the surface subarctic gyre (Figure 7b), which is similar to the slope previously observed at high latitudes, as exemplified in the Ross Sea (e.g., 37.6 μM M^{-1}) [*Saito et al.*, 2010]. The DCo:P slopes did not vary significantly in surface waters of the SAG despite a southward decrease of DCo concentrations (Figures 4a and 8b). Diatoms may dominate the phytoplankton assemblage at the highest latitudes of the SAG [*Parsons and Lalli*, 1988], whereas coccolithophorids

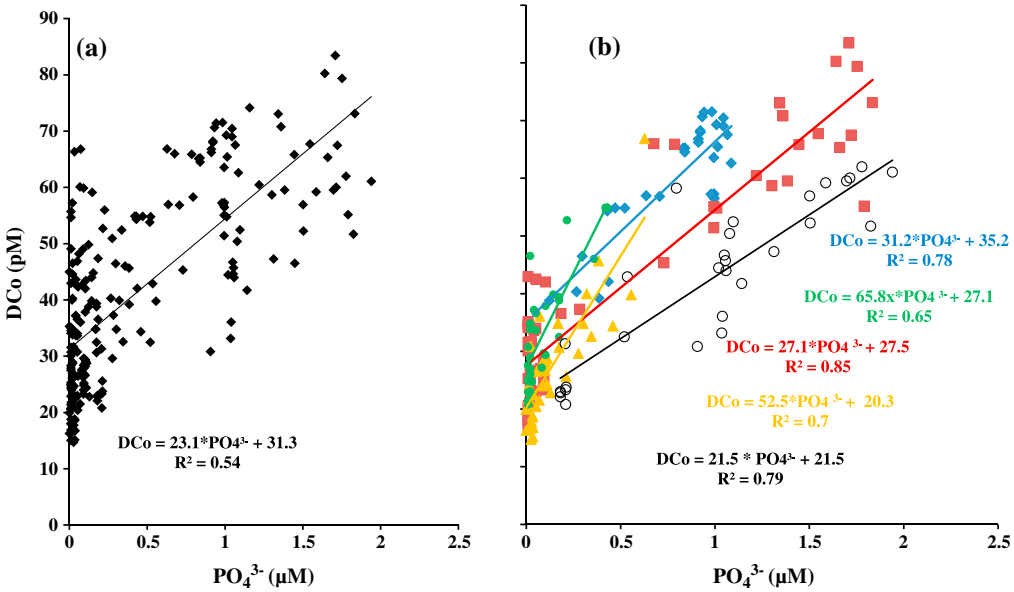

Figure 8. Scatter plots of the DCo data versus phosphate in the upper 250 m, showing (a) the global DCo-P relationship ($n = 228$) along the section and (b) the regional DCo-P relationships obtained in the SAG ($n = 28$; blue diamonds), the NASG ($n = 32$; green dots), the equatorial area ($n = 53$; red squares), the SASG ($n = 51$; yellow triangles), and the SAW ($n = 22$; white dots).

were probably blooming in the southern side of this domain during spring [*Okada and McIntyre*, 1979; *Head et al*., 2000; *Gregg and Casey*, 2007]. Diatoms have a lower cellular Co:P quota (60–150 µM M^{-1}) compared to coccolithophorids (300–360 µM M^{-1}) [*Ho et al*., 2003; *Cullen et al*., 2003; *Tang and Morel*, 2006; *Twining et al*., 2011] that have an higher biological requirement for Co [*Sunda and Huntsman*, 1995]. In turn, it is possible that strong biological uptake of DCo (and P) by blooming coccolithophores could have caused the depletion of DCo observed in the southern section of the SAG. The invariance of the DCo:P slope in this domain suggests that additional processes, such as the lateral advection, may account for the observed correlation. The seasonal decrease of the DCo surface concentrations observed in this area between April 2010 ($DCo_{\int upper\ 250m} = 66$ pM at station 6-58.6°N) and August 2012 ($DCo_{\int upper\ 250m} = 55.1$ pM at station 3c-57.2°N, Figure 6a) fits with the observed formation of the shallow pycnocline or thermocline at the end of spring which can promote the coccolithophorid bloom [*Head et al*., 2000].

At the high latitudes of the Southern Hemisphere, the lowest DCo:P slope of 21.5 µM M^{-1} ($R^2 = 0.79$; $n = 22$; Figure 8b) was observed in the subantarctic waters. This slope might reflect the low Co:P cellular quota of diatoms [*Twining et al*., 2011] which probably dominate in this area [*Ferreira et al*., 2013; *Browning et al*., 2014]. In addition, the high productivity of this area [*Field et al*., 1998] may have significantly reduced the DCo stock close to the MBC (Figure 4a), in spite of a low Co biological requirement by diatoms [*Sunda and Huntsman*, 1995]. A southward shift between the surface gradient of DCo and dissolved zinc (DZn) in subantarctic waters [*Croot et al*., 2011; Middag et al., unpublished data, 2014] suggests a southward decrease of DCo uptake by diatoms when DZn becomes nonlimiting. Indeed, diatoms are known to preferentially assimilate Zn compared to Co [*Sunda and Huntsman*, 1995].

The equatorial domain was characterized by a low DCo:P slope of ~27 µM M^{-1} ($R^2 > 0.87$; $n = 51$; Figure 8b). It contrasts with the extremely high DCo:P slope (>560 µM M^{-1}) reported at similar latitudes but in the central Atlantic [*Saito and Moffett*, 2002]. However, it may be difficult to compare these ratios since the latter was obtained with subsurface samples (5 m depth only), and close to the African coast. In that area, DCo probably accumulated at the subsurface notably due to dust dissolution, which would increase the DCo:P slope. In the western equatorial region, the plankton assemblage could be dominated by both the cyanobacteria *Richelia intracellaris* and the diatom *Pseudonitzschia* during summer (June and July) [*Tovar-Sanchez et al*., 2006]. The DCo:P slope recorded in this area (27.1 µM M^{-1}) was similar to the cellular Co:P mean quota determined for the bulk of these species (31 µM M^{-1}) [*Tovar-Sanchez et al*., 2006]

suggesting that the biological uptake of DCo and P by cyanobacteria and diatoms can drive their concentrations and ratio. The low DCo:P observed in the surface waters of the equatorial domain may also be accounted for by vertical diffusion fluxes from intermediate waters of relatively low DCo:P (23.1 $\mu M\,M^{-1}$ between 250 and 600 m depths) [*Dulaquais et al*., 2014].

The highest DCo:P slopes were observed in the subtropical areas (Figure 8b), with the highest mean value being observed in the Sargasso Sea (DCo:P $> 65.8\ \mu M\,M^{-1}$; $R^2 > 0.65$; $n = 32$; Figure 8b). Combined with the low DCo concentrations recorded (Figure 4a), it suggests strong biological uptake of DCo in the subtropical provinces. The ratios observed in this study were in the same range, although slightly higher, than those previously reported in other oligotrophic regions [*Saito and Moffett*, 2002; *Noble et al*., 2008; *Jakuba et al*., 2008; *Bown et al*., 2011; *Twining and Baines*, 2013]. The cyanobacteria *Prochlorococcus* sp. and *Synechococcus* sp., *which* dominate the picophytoplankton assemblage in oligotrophic regions,have an absolute cobalt requirement for growth [*Saito et al*., 2002] and thus assimilate Co leading to the low DCo concentrations recorded in these domains (Figure 4a). Furthermore, the high DCo:P observed in these oligotrophic waters are consistent with the high Co:P cellular ratios reported in phytoplankton bulk dominated by *Prochlorococcus* sp. and *Synechococcus* sp. from the eastern Atlantic (e.g., 260 $\mu M\,M^{-1}$) [*Tovar-Sanchez et al*., 2006].

Significantly lower P concentrations were recorded in the NASG (mean 0.07 μM) compared to the SASG (mean 0.19 μM) in the upper 250 m. The alkaline phosphatase activity of the biota could be enhanced at nanomolar concentrations of P [*Ji and Sherrell*, 2008], as reported in the Sargasso Sea. and thus, the biological uptake of DCo would also be higher [*Sunda and Huntsman*, 1995; *Jakuba et al*., 2008]. Thus, it is possible that Co was used more intensely in the NASG, likely contributing to the higher DCo:P there (65.8 $\mu M\,M^{-1}$) compared to the SASG (52.5 $\mu M\,M^{-1}$). The higher atmospheric input of Co in the Northern Hemisphere (Figure 10) also likely caused an accumulation of DCo relative to P in the NASG (Figure 4c) and thus higher DCo:P ratios.

Overall, the regional DCo:P slopes were generally lower than Co:P cellular ratios of the dominant phytoplankton species suggesting that other processes were occurring in addition to biological uptake in surface waters.

4.1.2. Biological Uptake and Regeneration Rate of Dissolved Cobalt in Surface Waters as Exemplified at the Bermuda Atlantic Time-Series Study Station

The cellular quotas of Co:P reported for the dominant phytoplankton functional groups potentially present in the different biogeochemical domains along the section were significantly higher than the corresponding DCo:P slopes we measured in the surface waters except in the equatorial region (Figure 8b) [*Ho et al*., 2003; *Cullen et al*., 2003; *Tang and Morel*, 2006; *Tovar-Sanchez et al*., 2006; *Twining et al*., 2011; *Twining and Baines*, 2013]. For instance, DCo:P in the upper 250 m of the Sargasso Sea (65.8 $\mu M\,M^{-1}$) was 4 times lower than the cellular Co:P quota of the predominant cyanobacteria (e.g., 260 $\mu M\,M^{-1}$; as reported in a bulk of *Prochlorococcus* sp. and *Synechococcus* sp. in the eastern Atlantic; *Tovar-Sanchez et al*. [2006]). Because the apparent biological use of DCo relative to P did not match the cellular quotas, the stoichiometric DCo:P slopes should thus reflect a combination of the several sinks and sources terms, such as regeneration in surface waters, in addition to the biological uptake. Hence, the DCo:P measured in the Sargasso Sea was used to discriminate the terms and to estimate the regeneration rate of DCo. The biological uptake rate of DCo by the cyanobacteria, that presumably dominate the phytoplankton assemblage in these waters, was estimated in the top 100 m (Table 2). The biomass was derived from the in situ Chl *a* (fluorescence) measurements, and literature values were used for growth rate of cyanobacteria in the Sargasso Sea and their Co/C cellular quota (equation (1) and references therein). We estimated a Co:C cellular quota of 2.16 $\pm 0.7\ \mu M\,M^{-1}$ for cyanobacteria, which is in agreement, considering the relative error, with the Co:C ratio reported in particulate matter of Sargasso Sea ($1.5 \pm 0.6\ \mu M\,M^{-1}$) [*Sherrell and Boyle*, 1992] and the Co:C cellular quota of *Synechococcus* sp. (1.43 $\mu M\,M^{-1}$) [*Sunda and Huntsman,* 1995] grown in zinc-depleted conditions similarly to surface waters of the Sargasso Sea [*Bruland and Frank*, 1983]. In our approach, the scavenging process could not be discerned from the biological uptake. The covariation between the relative proportion of PCo and the Chl *a* concentration we observed in the upper 1000 m along the section (Figure 5) strongly suggests that the transfer of DCo to PCo could be mainly driven by biological processes rather than by scavenging onto particles. Thus, the scavenging rate of DCo ($FDCo_{scavenging}$) was assumed negligible in

Table 2. Summary of Dissolved Cobalt (FDCo) and Phosphorus (FP) Fluxes Integrated for the Upper 100 m at the BATS Station in the Sargasso Sea[a]

	Atmospheric Deposition[b]	River Input	Lateral Advection[c]	Vertical Diffusion[c]	Scavenging[d]	Uptake	Regeneration
FDCo (nmol m^{-2} d^{-1})	+ 0.7 ± 0.1	Negligible	+ 0.08 ± 0.01	+ 0.05 ± 0.01	Negligible	− 45 ± 15	+ 37 ± 15
FP (μmol m^{-2} d^{-1})	+ 0.14 ± 0.03	Negligible	+ 0.02 ± 0.01	+ 0.72 ± 0.1)	Negligible	− 175 ± 53	+ 61 ± 18

[a]Standards errors are indicated in brackets.
[b]See section 4.2.2 for the calculation.
[c]From and following the method of *Dulaquais et al.* [2014] with the following: $FDCo_{diffusion} = -(K_z + D_T) \times (\partial DCo/\partial z)$ and $FDCo_{adv} = GradDCo_{(x,y)} \times velocity_a \times z$.
[d]Scavenging could not be discerned from biological uptake.

the surface waters. This assumption is further supported by a previous study that also suggests absence o scavenging in the upper waters column of Sargasso Sea [*Moffett and Ho*, 1996].

$$FDCo_{uptake} = (Co/C)_{cyano} \times (C/Chl\ a) \times 1/M_C \times [Chl\ a]_{\int 100m} \times \mu \quad (1)$$

where $(Co/C)_{cyano} = 2.16\ \mu mol\ mol^{-1}$ using $(Co/P)_{cyano} = 260\ \mu mol\ mol^{-1}$ [*Tovar-Sanchez et al.,* 2006] and $(P/C)_{cyano} = 8.3 \pm 2.6\ mmol\ mol^{-1}$ (after the review by *Bertilsson et al.* [2003]); μ is the growth rate of cyanobacteria in the Sargasso Sea and it is equal to 0.4 day^{-1} [*Mann*, 2000]; C/Chl *a* = 75 g g^{-1} [*Arrigo et al.*, 1998]; and Mc is the carbon molar mass (12 g mol^{-1}).

These calculations lead to an uptake flux of DCo of 45 ± 15 nmol DCo m^{-2} d^{-1} by the cyanobacteria at the Bermuda Atlantic Time-series Study (BATS) station (Table 3), which is in agreement with an estimate by *Saito et al.* [2002] for the upper 100 m of the Sargasso Sea (30 ± 12 nmol DCo m^{-2} d^{-1}). The apparent slope of DCo versus P ($\Delta DCo/\Delta P_{app}$) reflects the sum of the fluxes $\sum F$ (sources and sinks) of DCo relative to that of P as in equation (2):

$$(\Delta DCo/\Delta P)_{app} = \sum F_{DCo} / \sum F_P \quad (2)$$

The DCo fluxes were estimated in the top 100 m at the BATS station (Table 2). The P fluxes were estimated using the same parameterization as for DCo, but using the P concentrations data (Table 2). In the Sargasso Sea, the regeneration rate of P ($FP_{reg.}$) was determined using a relationship between regeneration and uptake fluxes of P ($FP_{reg..} = -0.35 \times FP_{uptake}$) [*McLaughlin et al.*, 2013]. Then using equation (2), the regeneration flux of DCo can thus be written as

$$FCo_{reg} = \left[(\Delta DCo/\Delta P)_{app} \times \sum F_P\right] - \left[FDCo_{diffusion} + FDCo_{advection} + FDCo_{atmosphere} + FDCo_{uptake} + FDCo_{scavenging}\right] \quad (3)$$

A DCo regeneration rate of 37 ± 15 nmol m^{-2} d^{-1} was estimated at BATS (Table 2), using the measured DCo/P slope at BATS of 69.2 μM M^{-1}. This regeneration flux represented about 80% of the Co uptake rate by cyanobacteria (e.g., $FCo_{reg.}/FCo_{uptake} = 0.8$), indicating that most of the biogenic cobalt can be recycled in these surface waters. A different approach resulted in similar estimates of 70–90% regeneration for oligotrophic waters of the southeastern Atlantic [*Bown et al.*, 2011]. From these calculations, we estimate a corresponding turnover of Co in cyanobacteria cell ($\tau_{Co\ cell} = FCo_{uptake}/FCo_{reg.}$) of 1.3 days at BATS.

In Sargasso Sea, the regeneration rate of P represented only 35% of its biological uptake in these waters (Table 2). The twofold difference in regeneration rates of P and DCo suggests non-Redfieldian regeneration of P and DCo and is probably the cause of the mismatch between the DCo:P slope and the Co:P cellular ratio in these waters. These estimates of biological DCo fluxes are based on estimated Co:C ratio in cyanobacteria; large uncertainty exists on this term, and further determinations will be required to improve such calculation of the bioassimilation and regeneration rate of DCo. The organic speciation of DCo also needs to be taken into account since it too can impact the bioavailability of DCo [*Saito et al.*, 2002; *Bown et al.*, 2012]. For instance, it has been suggested that *Prochlorococcus* sp. are able to assimilate organically bounded DCo [*Saito et al.*, 2002] and that cyanobacteria might produce organic binding-DCo ligands in oligotrophic waters [*Bown et al.*, 2012].

Table 3. Cobalt to Organic Carbon Ratio in Particles at 100 m Derived From Measurements ($PCo_{>0.2\mu m}/POC_{>1\mu m}$), and the Integrated Export Fluxes of Co on Large Particles (>53 μm) at 100 m (FCo_{export})[a]

	Domain					
	SAG	NASG	N-EA	S-EA	SASG	SAW
$PCo_{>0.2\mu m}/POC_{>1\mu m}$ (μM M^{-1})	2.1 ± 0.6	6.9 ± 1.4	1.5 ± 0.4	1.5 ± 0.4	2.16[b]	0.4[b]
FCo_{export} (nmol m^{-2} d^{-1})	4.2 ± 3.4	12.9 ± 32.4	3.6 ± 2.0	5.5 ± 1.5	4.9 ± 1.2	2.3 ± 0.5

[a]N-EA: North Equatorial area; S-EA: South Equatorial area.
[b]Data from *Bown et al.* [2011].

4.1.3. Export of Cobalt From the Surface Waters

The export flux of cobalt on settling particles from the surface waters was estimated using the export fluxes of the particulate organic carbon (POC) at 100 m depth (C_{export}, equation (4)) inferred from $^{234}Th/^{238}U$ measurements ($^{234}Th_{flux}$) in the water column and the $POC/^{234}Th$ ratio measured in large particles >53 μm [*Owens et al.*, 2014; V. Puigcorbé et al., manuscript in preparation, 2014]. The Co:C ratio was found to covary in large and total particles ($n = 5$) in the northwestern Atlantic (at 35.4°N–66.5° and 39.7°N–69.8°W) during the GEOTRACES-A03 cruise (Phoebe Lam, personal communication, 2014). This allows us to use equation (5) and to calculate the export fluxes of Co by the large settling particles (>53 μm) at 100 m (FCo_{export}, equation (6)).

$$C_{export} = {}^{234}Th_{flux} \times \left(POC_{>53\mu m}/{}^{234}Th\right) \quad (4)$$

$$PCo_{>53\mu m}/\ POC_{>53\mu m} = PCo_{>0.2\mu m}\ /\ POC_{>1\mu m} \quad (5)$$

$$FCo_{export} = C_{export} \times \left(PCo_{>53\mu m}/\ POC_{>53\mu m}\right) \quad (6)$$

In the Northern Hemisphere, the carbon export fluxes were available at date for 14 stations at 100 m depth (Puigcorbé et al., manuscript in preparation), and mean values of the Co: POC ratios were estimated in the SAG, the NASG, and the Equatorial Area (EA) (Table 3). In the Southern Hemisphere, the carbon export fluxes were available at 18 stations at 100 m depth [*Owens et al.*, 2014] but there was no POC data available in the SASG and the SAW. For these domains, PCo/POC ratios recorded in similar biogeochemical conditions in surface waters (e.g., *T*, Chl *a*, DCo) but in the southeastern Atlantic [*Bown et al.*, 2011] were used (Table 3).

In the subarctic gyre and the equatorial area, the PCo/POC ratios were, respectively, equal to 2.1 ± 0.6 and 1.5 ± 0.4 μM M^{-1} at 100 m depth. These values are in excellent agreement with the Co/C cellular quota of coccolithophorids in nonlimiting conditions (1.4–3.6 μM M^{-1}) [*Sunda and Huntsman*, 1995; *Ho et al.*, 2003] but much higher than those measured in oceanic diatoms (0.3 μM M^{-1}) [*Twining et al.*, 2011]. At 23°N, the PCo/POC ratio (6.9 ± 1.3 μM M^{-1}) was 3 times higher than the cellular quota of the predominant cyanobacteria (1.43–2.16 μM M^{-1}) [*Sunda and Huntsman*, 1995; *Tovar-Sanchez et al.*, 2006] and than the PCo/POC ratio obtained in particulate material collected with in situ pumps in oligotrophic conditions (1.5 ± 0.6 μM M^{-1}) [*Sherrell and Boyle*, 1992], suggesting an additional (lithogenic) source of PCo in these waters probably from the atmosphere as shown below. In the SASG, the PCo/POC ratio used (2.15 μM M^{-1}) [*Bown et al.*, 2011] was in the range of the cellular quota of cyanobacteria [*Sunda and Huntsman*, 1995; *Tovar-Sanchez et al.*, 2006]. South of the Southern Subtropical Front, the PCo/POC ratio of 0.4 μM M^{-1} (derived from *Bown et al.* [2011]) was in agreement with the cellular quota of diatoms [*Twining et al.*, 2011] that probably dominate the phytoplankton assemblage in this area [*Browning et al.*, 2014].

The estimated export flux of Co varied within the different biogeochemical domains (Table 3), with the lowest in the SAW (2.3 ± 0.5 nmol m^{-2} d^{-1}; $n = 6$) and the highest in the NASG (13 ± 32 nmol m^{-2} d^{-1}; $n = 6$). Interestingly, relatively lower Co export fluxes were estimated in domains with potentially higher particulate sinking rates such as the SAW and the north EA, due to the predominance of diatoms, compared to areas like the NASG that are dominated by cyanobacteria and have nominally lower particulate sinking rates (Table 3). This suggests that the export of Co by particles might not be directly proportional to the primary productivity, and that other parameters should be taken into account such as the biological requirement and uptake of Co by the dominant functional groups that can drive the Co

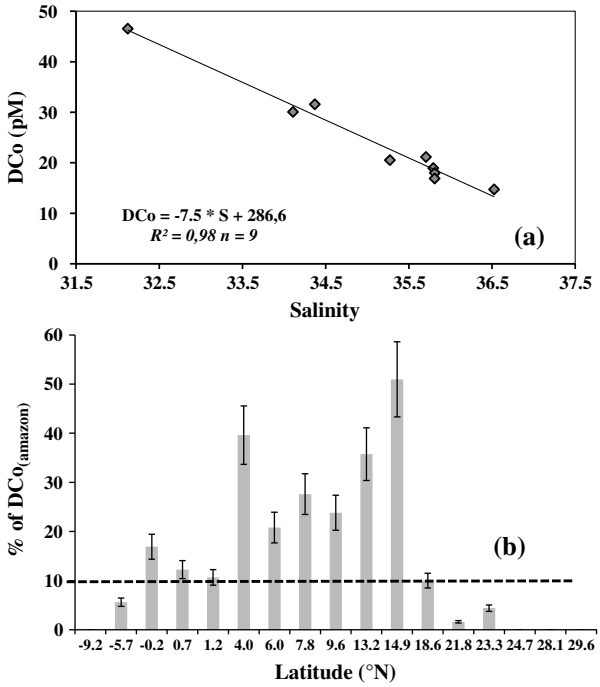

Figure 9. (a) Inverse linear correlation ($R^2 > 0.97$) between dissolved cobalt (DCo) and the salinity in the waters influenced by the discharge of the Amazon (dark stars). (b) Percentage of the DCo stock in the mixed layer attributed to the input by the Amazon. The dashed line indicates 10% contribution of the Amazon to the DCo stock.

abundance in the exported biogenic particles. This result contrasts with previous assumptions suggesting that the POC export could be rather small in oceanic domains dominated by the picoplankton and nanoplankton [*Takahashi and Bienfang*, 1983; *Silver et al*., 1986; *Goldman*, 1988, 1993]. However, it is in line with recent findings showing that *Synechococcus* sp., *Prochlorococcus* sp., and nanoplankton can represent a significant portion of the POC downward flux especially in the oligotrophic regions, contributing to up to 33 ± 16% of the POC export flux in the Sargasso Sea [*Lomas and Moran*, 2011]. In turn, the absolute requirement of cyanobacteria for Co associated with the atmospheric deposition, as discussed in the following section, below could account for the enrichment of large particles in Co and therefore for the high export flux of Co estimated in the NASG.

4.2. External Sources of Dissolved Cobalt in the Western Atlantic

4.2.1. The Input by the Amazon

With a mean water flux of 172 000 $m^3 s^{-1}$ [*Molleri et al*., 2010], the Amazon River represents an important source of many elements to the western equatorial Atlantic [*Boyle et al*., 1982; *Aucour et al*., 2003; *Seyler and Boaventura*, 2003] and its influence has been traced as far as the Caribbean basin [*Moore et al*., 1986]. In contrast, it has a little impact on regions south of the equator and east of 47°W [*Molleri et al*., 2010] due to the direction of its plume. However, retroflection of the North Brazil Current and the equatorial countercurrent can transport signatures of the plume southeastwards of its mouth [*Molleri et al*., 2010].

A strong linear correlation between DCo concentrations and salinity of 32 to 36.5 was found in the plume of the Amazon ($R^2 > 0.97$, $n = 9$; this study; Figure 9a). At the extrapolated zero salinity, the DCo concentration was thus estimated at 287 pM (Figure 9a). This end-member estimate is significantly lower than the DCo concentration of 0.64–1.87 nM reported for the upper Amazon [*Seyler and Boaventura*, 2003]. Similarly, underestimation of the DCo end-member for a North American estuary has already been reported [*Saito and Moffett*, 2002]. Transfer from dissolved to particulate fractions through chemical flocculation [*Church*, 1986; *Moffett and Ho*, 1996] can explain the difference between the reported and estimated end-members. The Co discharge to the estuary of the Amazon has been shown to predominantly occur as particulate cobalt, representing up to 95% of the total Co discharge [*Seyler and Boaventura*, 2003]. It is thus conceivable that the increase of the ionic strength across the saline gradient would cause flocculation and particles precipitation that would trap much of the riverine input in the delta sediments [*Smoak et al*., 2006]. On the other hand, sediments are subjected to constant reworking, such as sediment resuspension and dissolution that would increase the DCo input from the estuary. Additional data are clearly needed across the saline gradient to understand the behavior of DCo in the Amazon plume. Biological drawdown, in addition to such flocculation processes and to the dilution of the plume, can also account for the decrease of DCo along the pathway of the plume. For instance, higher intracellular Co-quotas of bacteria growing in the plume of the Amazon were reported compared to those of species growing outside it [*Tovar-Sanchez and Sañudo-Wilhelmy*, 2011], suggesting higher biological uptake of DCo in the Amazon plume.

In order to estimate the input of DCo from the Amazon to our study region, we used the first-order DCo-salinity relationship (Figure 9a; $\Delta DCo/\Delta S = -7.5$ pM). Then we normalized the relationship assuming the Amazon influence is null for $S \geq 36.5$ (equation (7)), since no plume was observed along the section at S above this value. The Amazon plume was depicted by its low salinities and its relatively high Si:N ratios observed in the mixed layer, consistent with previous observations [*Hellweger and Gordon*, 2002]. We estimated the concentration of DCo brought by the Amazon (DCo_{Amazon}) and its relative contribution (% DCo_{Amazon}, Figure 9b) to the mean DCo concentration recorded in the mixed layer (DCo_z), according to

$$DCo_{Amazon} = (S_{obs} - 36.5) \times \Delta DCo/\Delta S \quad (7)$$

$$\%\ DCo_{Amazon} = DCo_{Amazon}/DCo_z \times 100 \quad (8)$$

Where S_{obs} is the observed salinity and varies from 32 to 36.5; z varied between 15 and 60 m.

The input of DCo by the Amazon was significant (>10%) for 10 stations ($DCo_{Amazon} > 10\%$ of DCo_z; Figure 9b), and varied between 2.2 ± 0.5 pM at 18°N (station 30) and up to 14.3 ± 2.9 pM at 15°N (station 32) where it accounted for 51% of the DCo_z. The advection of DCo by the plume of the Amazon River was detectable until 18°N (between station 18b and 30; Figure 9b), whereas northward, it was considered negligible as it represented less than 10% of the DCo_z. The contribution southward of the Amazon mouth was also found to be negligible. These estimates suggested that the DCo inputs by the Amazon discharge can be significant in the northwestern tropical Atlantic between the equator and 18°N (Figure 9b).

In fact, the inputs of nutrients by the Amazon River might significantly promote the diazotrophy in the central western Atlantic, as it has been previously suggested [*Subramaniam et al*., 2008]. It has been shown that up to 100% of the cellular metal content (including Co) of the diazotroph *Trichodesmium sp.* growing in the Amazon plume of the central Atlantic may actually originate from the Amazon discharge [*Tovar-Sanchez et al*., 2006]. These cyanobacteria are producers of B_{12}-vitamin that requires Co as the central atom [*Bonnet et al*., 2010] and B_{12} production could be enhanced by input of DCo [*Panceza et al*., 2008]. The production of B_{12}-vitamin may also promote the development of several other phytoplankton species limited by this vitamin [*Bertrand et al*., 2007; *Bonnet et al*., 2010], when iron is not limiting as likely it was the case in these waters [*Rijkenberg et al*., 2014]. In turn, the input of DCo by the Amazon in the north equatorial area could have ecological implications through an Amazon-DCo-B_{12} cascade.

4.2.2. The Atmospheric Contribution

Several subsurface DCo maxima ($DCo_{10m} > DCo_{25m}$) were observed along the section in the Northern Hemisphere, especially in the NASG and in the northern equatorial area (Figures 6b and 6c). Moreover, relative maxima of PCo were generally observed in the upper 50 m along the transect (Figure 4b). The highest surface concentrations of PCo were recorded in the NASG, representing 10–20% of the TCo in subsurface, and up to 34% at 26°N (e.g., $PCo = 10.3 \pm 2.6$ pM at 25 m), whereas this fraction only represented generally less than 2% of the TCo concentration below 400 m. These observations suggested a possible atmospheric deposition of PCo in the NASG that produced subsurface DCo maxima after dissolution. In addition, anomalies of high DCo:P ratios (up to > 5.4 mM M^{-1}) were observed in the surface waters of the NASG centered at 23°N and the equatorial area (Figure 4c), likely resulting from an accumulation of DCo versus P. Indeed, the Co:P ratio in aerosols is significantly higher than in seawater ($Co:P_{seawater} < 10^{-3}$ M.M^{-1}, this study; $Co:P_{aerosols} > 10^{-2}$ M.M^{-1}, *Reid et al*. [2003]). Therefore, dissolution of aerosols might have caused these high DCo:P ratio. Additionally, the relative accumulation of DCo (versus P) was associated with an enrichment of dissolved aluminium (DAl) (Middag et al., unpublished data) in these surface waters (Figure 4c), further suggesting dust inputs in this region, far away from other potential external sources. Previous observations have shown that dust can be transported from North Africa to the entire tropical Atlantic all yearlong [*Prospero and Lamb*, 2003]. Using a modified dust deposition MADCOW model based on DAl as proxy for the dust input [*Measures and Brown*, 1996; *Measures and Vink*, 2000; *Vink and Measures*, 2001; *de Jong et al*., 2007] and the surface DAl concentrations recorded along the section (Middag et al., unpublished data), we estimated dust deposition rates in the western Atlantic. Improvements in this model are inclusion of variable

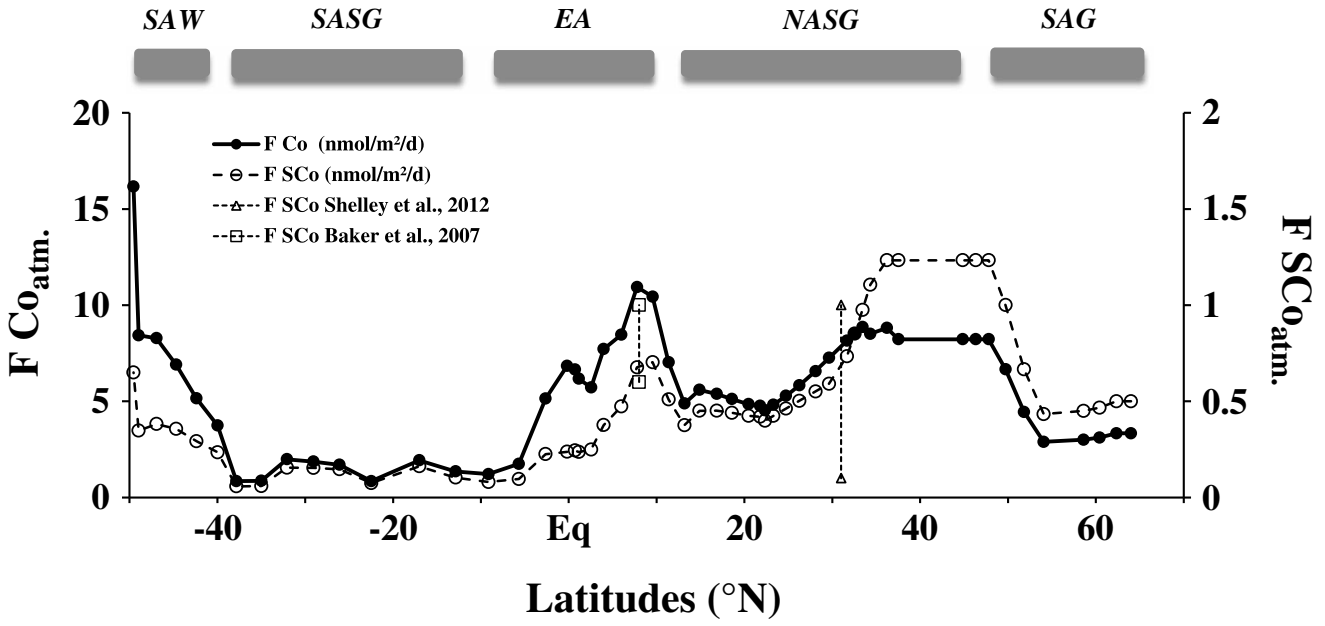

Figure 10. Estimation of the sea surface atmospheric deposition of dry (dark circles, solid line) and soluble (open circles, dashed line) cobalt, along the section. The soluble Co deposition estimated by *Shelley et al*. [2012] and *Baker et al*. [2007] are shown for comparison.

mixed layer depth, variable Al solubility of aerosols, and variable DAl residence times. The residence time of DAl in surface waters was assessed from its scavenging flux (equation (9); see supporting information for the parameterizations and coefficients). Dust deposition fluxes ranged from less than $0.20 \pm 0.04\ g\ m^{-2}\ yr^{-1}$ at several stations in the SASG (stations 7, 8, 9, and 10) to up to $5.4 \pm 1.1\ g\ m^{-2}\ yr^{-1}$ at about 8°N (station #36).

Despite the difficulties and limitations to use DAl as a dust proxy [*Dammshäuser et al*., 2011], especially due to its removal through biogenic particles [*Moran and Moore*, 1988; *Middag et al*., 2009], our estimations are consistent with previous studies showing that the atmospheric input can be 10 times higher in the NASG than in the SASG [*Tegen et al*., 2004; *Jickells et al*., 2005], and with model predictions of dust deposition in the Atlantic Ocean [*Ginoux et al*., 2001; *Tegen et al*., 2004; *Mahowald et al*., 2005: *van Hulten et al*., 2013] (see supporting information).

$$\text{Dust deposition rate} = \text{DAl} \times z \times M\ \text{Al} \times (\text{Ab Al} \times \text{S Al} \times \tau\ \text{Al})^{-1} \quad (9)$$

where DAl is the mean dissolved aluminum (Al) concentration in the mixed layer, z is the mixed layer depth, M Al is the molar mass of aluminum, Ab Al is the crustal abundance of Al, S Al is the solubility of Al in aerosols [from *Baker et al*., 2013], τAl is the residence time of Al in the mixed layer (see supporting information for parameterizations and coefficients).

Considering these estimated rates of dust deposition, and the concentrations of Co in dust ($[Co]_{dust}$) that varied from 17 to 170 $\mu g\ g^{-1}$ in aerosols of the West Atlantic depending of their origins [*Gaiero et al*., 2003; *Reid et al*., 2003; *Rudnick and Gao*, 2003; *Baker et al*., 2007; *Trapp et al*., 2010; *Xia and Gao*, 2010; *Shelley et al*., 2012; R. Shelley, personal communication, 2014] (see supporting information), we estimated the atmospheric Co deposition flux (Flux Co_{atm}) along the section, according to equation (10):

$$\text{Flux Co}_{atm.} = \text{Dust deposition rate} \times [\text{Co}]_{dust} \quad (10)$$

The estimates of Co deposition rates varied from 0.9 $nmol\ m^{-2}\ d^{-1}$ in the center of the SASG to up to 17.4 $nmol\ m^{-2}\ d^{-1}$ close to Patagonia (station 1b) (Figure 10). The strongest deposition of dust was centered on the EA (see supporting information), whereas the relatively high atmospheric inputs of Co were located in the temperate latitudes of the Northern Hemisphere (35°N–50°N; mean Flux $Co_{atm} = 8 \pm 1\ nmol\ m^{-2}\ d^{-1}$),

the northern equatorial area (mean Flux $Co_{atm} = 8 \pm 2$ nmol m^{-2} d^{-1}) and away from Patagonia in the SAW (mean Flux $Co_{atm} = 9 \pm 4$ nmol m^{-2} d^{-1}). Much lower Co atmospheric depositions were found in the SASG (mean Flux $Co_{atm} = 1.5 \pm 0.5$ nmol m^{-2} d^{-1}) and the SAG (mean Flux $Co_{atm} = 3 \pm 1$ nmol.m^{-2}.d^{-1}). The high atmospheric deposition of Co in the EA was linked to the high dust deposition, and those estimated in the SAW and at temperate latitudes of the North Atlantic to the Co enrichment of, respectively, the Patagonian aerosols [*Gaiero et al*., 2003] and the North American aerosols (R. Shelley, personal communication). Low Co atmospheric inputs were mainly caused by low dust depositions.

The atmospheric input of soluble Co (Flux $SCo_{atm.}$) was then estimated using solubility coefficients of Co from dust, following equation (11).

$$\text{Flux } SCo_{atm.} = FCo_{atm} \times S\ Co \tag{11}$$

where *S* Co is the dissolution coefficient of cobalt from atmospheric particles in seawater and varies from 3% to 15% depending of the origin of the aerosol (see supporting information for the coefficients).

The modeled atmospheric deposition of soluble Co showed a different pattern compared to the estimated input of TCo (Figure 10). The highest input of soluble Co was indeed located in the temperate northern Atlantic, where 10 times higher inputs of soluble Co were estimated compared to the SASG (Figure 10). The model also showed a strong asymmetry of the soluble Co inputs between the two hemispheres with higher *F* SCo_{atm} in the north with the exception of the SAW where inputs from Patagonia are detected (Figure 10).

Despite consistent trends, these estimations have to be taken carefully due to the lack of available data on the different parameters, especially on the solubility of aerosols in seawater. Moreover, seasonal differences in the intensity of the dust deposition and in the air masses regimes likely introduce seasonal differences in Co inputs. For instance, lower dust deposition can occur during fall than in summer [*Prospero and Lamb*, 2003]. We compared the accuracy of our estimates in the West Atlantic with the only two direct measurements of the atmospheric inputs of soluble Co available in the literature at date. At the BATS station (31°N), our estimate of soluble Co deposition (0.7 nmol m^{-2} d^{-1}) is in the range of the atmospheric DCo input previously measured during the FeATMISS-1 and FeAST-6 cruises (1.1 (late summer) and 0.1 nmol (early summer) m^{-2} d^{-1}, respectively; Figure 10) [*Shelley et al*., 2012]. At about 8°N, our estimation (0.7 nmol m^{-2} d^{-1}; Figure 10) was in agreement with the atmospheric inputs of soluble Co recorded in this area during fall by *Baker et al*. [2007] (0.6–1.1 nmol m^{-2} d^{-1}). Overall, our estimations strongly suggested that the atmospheric input can be a main external source of DCo in the subtropical and equatorial areas of the northwestern Atlantic. The asymmetry of $SCo_{atm.}$ inputs between the two hemispheres may be due to the westward trade winds that are strongest at the equator and 30°N compared to the south, and to the North American aerosols that can be enriched in Co at temperate latitudes (R. Shelley, personal communication). The higher inputs of soluble Co in the Northern Hemisphere can account for the relative accumulation of DCo (versus P) observed in the surface waters of the NASG (Figure 4c). Without the atmospheric input, the concentrations of DCo in the surface waters of the NASG would be similar to those recorded in areas receiving far less atmospheric inputs, such as in the SASG (e.g., 24 ± 5 pM) and in another oligotrophic gyres like in the Central Pacific [*Noble et al*., 2008] and the South Central Atlantic [*Noble et al*., 2012]. The biogeochemical implications of the atmospheric source of DCo are discussed in details elsewhere (G. Dulaquais and M. Boye, Atmospheirc cobalt deposition along the surface western Atlantic and biogeochemical implications, in review for publication in *Earth and Planetary Sciences Letters*).

4.3. Residence Time of Cobalt in the Upper 100 m Along the Western Atlantic

The residence time of dissolved (DCo) and particulate (PCo) cobalt in the upper 100 m of the different domains were inferred using the stocks measurements and estimates of sources and sinks fluxes we estimated (Table 4). It is conceptualized in a simplistic scheme of the Co cycling shown in Figure 7. The particulate export flux of Co (Table 2) was used to estimate the residence time of PCo in surface waters (equation (12)).

$$\tau\ \text{PCo} = \text{PCo stock} \times \text{Co export rate}^{-1} \tag{12}$$

The residence time of DCo due to biogeochemical processes (τDCo_{biogeo}, Table 4) was estimated considering the loss of DCo from the upper 100 m due to the export of the biogenic fraction of PCo (equation (13)).

Table 4. Stock and Residence Time of Dissolved (DCo) and Particulate (PCo) Cobalt in the Upper 100 m for the Different Biogeochemical Domains[a]

	SAG	NASG	N-EA	S-EA	SASG	SAW
PCo stock (μmol m^{-2})	0.93 ± 0.47	0.60 ± 0.34	0.52 ± 0.34	0.27 ± 0.17	0.11 ± 0.03	0.31 ± 0.19
τPCo (year)	0.6 ± 0.5	< 0.1 ± 0.1	0.4 ± 0.2	0.1 ± 0.1	< 0.1 ± 0.1	0.3 ± 0.2
DCo stock (μmol m^{-2})	5.9 ± 1	3.3 ± 0.8	3 ± 1	3.4 ± 1.0	2.4 ± 0.5	3.8 ± 0.8
$\tau DCo_{biogeo.}$ (year)	12.1 ± 6.1	1.4 ± 1.2	∞	3.4 ± 0.5	1.7 ± 0.5	∞
$\tau DCo_{phy.}$ (year)	0.7 ± 0.2	9.0 ± 2.2	1.0 ± 0.3	0.9 ± 0.3	6.6 ± 1.4	0.7 ± 0.2
$\tau DCo_{bio.}$ (year)[b]	0.2	0.1	0.3	0.3	0.1	0.5

[a]The residence times of DCo are given considering biogeochemical processes ($\tau DCo_{biogeo.}$) and physical processes ($\tau DCo_{phy.}$) (see text for the explanation and calculation). The biological transfer time of the DCo stock ($\tau DCo_{bio.}$) is also indicated.
[b]Estimated by τDCo_{bio} = DCo stock/DCo uptake (using DCo uptake from Table 5).

For the calculations, we assumed that the atmosphere was the only source of lithogenic PCo and that scavenging do not occurs in the upper 100 m. In a steady state regime, the export of the biogenic fraction of PCo can then be determined using equations (14) and (15).

$$\tau\ DCo_{biogeo} = DCo\ stock \times Co_{biotic}export\ rate^{-1} \quad (13)$$

$$Co_{biotic}export\ rate = Co\ export\ rate - Co_{lithogenic}export\ rate \quad (14)$$

$$Co_{lithogenic}export\ rate = FCo_{atm} - FCo_{sol} \quad (15)$$

The residence time of DCo due to physical processes (τDCo_{phy}, Tables 4) was also estimated following equation (16). The smaller of the two estimations will be considered as the residence time of DCo.

$$\tau\ DCo_{phy} = DCo\ stock \times (FDCo_{advection} + FDCo_{diffusion})^{-1} \quad (16)$$

The residence times of particulate cobalt in the surface waters were generally much lower than those of the dissolved cobalt in the different domains, up to 28 times lower in the SASG (Table 4). Particulate cobalt resided shortly in the two oligotrophic domains (τPCo ~20 days), whereas at high latitudes and near the equator, longer PCo residence times were estimated, up to 200 days in the SAG. In this later domain, the residence time of PCo was probably overestimated, as we assumed a steady state, whereas an intensive bloom occurring during our period of sampling (spring) may have increased the PCo stock by the assimilation of DCo. This would result in the apparent high stock of PCo (~1 μmol m^{-2}) that might not be representative of the annual average PCo stock.

The longer residence times of DCo were estimated in the two oligotrophic domains (~1.5 years). In these high-regeneration systems, the residence times of DCo were driven by biogeochemical processes rather than by the physical processes ($3 < \tau DCo_{phy}/\tau DCo_{biogeo} < 7$). On the contrary, at high latitudes the physical processes may drive the DCo residence time ($0 < \tau DCo_{phy}/\tau DCo_{biogeo} < 0.06$). Similar low-DCo residence times were estimated in the two hemispheres at high latitudes (0.7 year). Advection of DCo-enriched waters by the Labrador Current in the north and by the Malvinas Current in the south and strong seasonal biological Co uptake may explain the short residence time at those high latitudes. On either sides of the equator, we estimated an intermediate residence time of ~1 year. Like at the high latitudes, the physics could drive the DCo residence time there, notably due to high-DCo input through diffusion caused by sharp vertical DCo gradients and by the equatorial current system that increases the diffusivity [*Dulaquais et al*., 2014]. Furthermore, the organic complexation of DCo in surface waters could slow down its scavenging onto particles [*Saito and Moffett*, 2001, 2002], further increasing its residence time in surface waters. The abundance of cyanobacteria in oligotrophic waters combined with their capacity to produce DCo organic ligands [*Saito et al*., 2005] would both account for the longer residence time of DCo estimated in these regions. Determination of the organic complexation of DCo in these waters is required to further confirm this hypothesis.

Table 5. Summary of the Dissolved (DCo) and Particulate (PCo) Cobalt Fluxes for the Upper 100 m (Averaging All Stations of Each Biogeochemical Domain) Along the GEOTRACES-A02 Section[a]

	Domain Period of Sampling	SAG Spring	NASG Dry Season	N-EA	S-EA	SASG Dry Season	SAW Summer
				Fluxes (nmol m^{-2} d^{-1})			
PCo (−) or DCo (+)	(1) Scavenging[b]	Negl.	Negl.	Negl.	Negl.	Negl.	Negl.
	(2) Uptake[c]	(−) 106 *[20–220]*	(−) 64 *[18–197]*	(−) 27 *[21–30]*	(−) 31 *[15–47]*	(−) 33 *[14–51]*	(−) 22 *[7–30]*
	(3) Regeneration[c]	10 *[2–50]*	51 *[14–130]*	21 *[16–23]*	11 *[5–20]*	28 *[10–40]*	7 *[2–10]*
	(4) Dust dissolution	0.5 *[0.4–0.6]*	1.0 *[0.3–1.3]*	0.5 *[0.2–0.7]*	Negl *[0.1–0.3]*	Negl *[0–0.2]*	0.5 *[0.3–0.7]*
PCo	(5) Dust	(+) 3 *[3–4]*	(+) 7 *[5–8]*	(+) 8 *[6–10]*	(+) 4 *[1–7]*	(+) 1.5 *[0.8–2]*	(+) 9 *[5–16]*
	(6) Export	(−) 4 *[3–5]*	(−) 13 *[0–30]*	(−) 4 *[2–6]*	(−) 6 *[5–8]*	(−) 5 *[3–7]*	(−) 2 *[1–3]*
	ΣFPCo	(+) 94.5	(+) 6.5	(+) 9.5	(+) 18	(+) 1.5	(+) 21.5
DCo	(7) Amazon[d]	Negl.	Negl.	(+) 1 *[0–4]*	Negl.	Negl.	Negl.
	(8) Vertical diffusion[e]	(+) 7 *[(−) 2–10]*	(+) 1 *[0–2]*	(+) 7 *[2–10]*	(+) 7 *[3–10]*	(+) 1 *[0–2]*	(+) 9 *[4–15]*
	(9) Lateral advection[f]	(+) 15	Negl.	(+) 2	(+) 4	Negl.	(+) 7
	ΣFDCo	(−) 73.5	(−) 11.5	(+) 4.5	(−) 9	(−) 4	(+) 2
				Basin Fluxes (t/yr)			
PCo + DCo	**Sum**[g]	(+) 380	(−) 970	(+) 330	(+) 190	(−) 160	(+) 280

[a] In italic and brackets = range, in bold = sum.
[b] Scavenging is assumed negligible.
[c] Using equations (1) and (3) with Co:C of 2.1 ± 0.6 μM M^{-1} in the SAG (this study); 2.16 ± 0.7 μM M^{-1} in the NASG and the SASG [after *Tovar-Sanchez et al.*, 2006; *Bertilsson et al.*, 2003]; 1.48 ± 0.4 μM M^{-1} in the N-EA and S-EA (this study); 0.4 μM M^{-1} in the SAW [*Bown et al.*, 2011].
[d] The Amazon flux of DCo is determined using $FDCo_{Amazon} = (DCo_{Amazon} \times z/100)/\tau DCo$.
[e] The diffusion fluxes are estimated as described in *Dulaquais et al.* [2014] and Table 3.
[f] The lateral advection of DCo is estimated in the SAG from ΔDCo concentrations between stations 2 and 13, an area of 8.4×10^5 km^2 and a mean water flow of 5 Sv in the upper 100 m [*Reid*, 1994; *Flatau et al.*, 2003]. In the SAW it is estimated from ΔDCo concentrations between stations 1b and 6b, an area of 5.5×10^5 km^2 and a mean water flow of 2.5–3 Sv in the upper 100 m [*Peterson et al.*, 1996]. In the N-EA, it is estimated from ΔDCo concentrations between stations 41 and 35, an area of 1×10^6 km^2 and a mean water flow of 5 Sv in the upper 100 m [*Tomczak and Godfrey*, 2003]. In the S-EA, it is estimated from ΔDCo concentrations between stations 15b and 41 an area of 1.1×10^6 km^2 and a mean water flow of 5 Sv in the upper 100 m [*Tomczak and Godfrey*, 2003].
[g] The sum is calculated using (Sum DCo + Sum PCo) × *S*, where *S* is the surface of the different domain (0.84 10^{12} m^2 for SAG, 9 10^{12} m^2 for NASG, 1.1 10^{12} m^2 for N-EA, 1 10^{12} m^2 for S-EA, 3 10^{12} m^2 for SASG, and 0.55 10^{12} m^2 for SAW).

In the northern subtropical domain, the residence time of DCo is 4 times higher than that previously estimated in the same area (e.g., 0.32 year) [*Saito and Moffett*, 2002]. However, it might be difficult to compare both values, since the latter was estimated without taking into account the regeneration process. Indeed, it was calculated as the quotient between the DCo stock and a mean annual new production of carbon at BATS [*Jenkins and Goldman*, 1985] that relies on a mean particulate Co:C ratio in the Sargasso Sea [*Sherrell and Boyle*, 1992]. On the other hand, our estimate of the biological transfer time of the DCo stock ($\tau DCo_{bio} = DCo_{stock}/FDCo_{uptake}$) at BATS (0.2 ± 0.1 year; Table 4) is in the range of the previous estimate of *Saito and Moffett* [2002]. In turn, the regeneration process increases the residence time of DCo in surface waters of Sargasso Sea.

Overall, these first assessments of the residence time of Co showed interesting features in the different domains. Longer PCo residence times were found in areas with shorter residence times of DCo and inversely, suggesting exchange processes between the two fractions. However, additional studies will be needed to better constrain these terms.

4.4. Comparative Budgets and Biogeochemical Cycling of Cobalt in the Surface Waters of the Western Atlantic

The Co budgets in the upper 100 m water layer of each biogeochemical province are presented in Table 5 for PCo and DCo and shown conceptually for the entire western Atlantic in Figure 11. These budgets represent the state of the system at the time of the observations; hence, they only integrate fluxes and processes operating with a timescale that allows their observations. The aim of this exercise is to compare the characteristics of the different domains and the order of magnitude of the different terms rather than determine absolute values. The budgets are based on the full data sets available during the cruises (chemical, biological, geochemical, and hydrographic parameters), but some fluxes had to be estimated using parameters from the literature when cruise data were lacking.

Biological assimilation was the dominant flux in the different biogeochemical domains (Table 5). This is in line with the observations showing an overall nutrient-like distribution of DCo in the surface waters (Figures 4 and 6). The biological uptake flux of DCo was estimated as mentioned above, using Chl *a* values derived from the in situ fluorescence measurements obtained during the cruises and reported values of cellular quotas of Co/C in the phytoplankton species (Table 5) dominating in the different biogeochemical provinces [*Sunda and Huntsman*, 1995; *Ho et al*., 2003; *Tovar-Sanchez et al*., 2006; *Twining et al*., 2011; *Twining and Baines*, 2013]. The lowest uptake was estimated for the SAW (22 nmol m^{-2} d^{-1}) and the highest in the SAG (106 nmol m^{-2} d^{-1}). In the latter domain a bloom of coccolithophorids was likely occurring during our period of sampling in 2010 as suggested by the relatively high Chl *a* and PCo levels (Figures 3d and 4b) and potentially accounting for this extremely high uptake rate of DCo. The reoccupation of the SAG at a different season showed a decrease of the DCo stock by 1.4 μmol m^{-2} (~25% of DCo stock) between April 2010 (station 8) and July 2012 (station 3c) at 57–58.6°N (Figure 6a). Considering the daily uptake of DCo estimated in the SAG during spring (106 nmol m^{-2} d^{-1}, Table 5), the observed DCo decrease (1.4 μmol m^{-2}) would correspond to 13 days of biological uptake. This fits with the timescale of a coccolithophorid bloom [*Brown and Yoder*, 1994], further supporting the idea that the surface DCo depletion observed in summer was related to a coccolithophorid spring bloom. The regeneration rate of DCo in the surface waters (Co_{reg}) was the second most important flux and represented between 10 and 85% of the Co uptake flux (Co_{uptake}; Table 5). The highest regeneration fluxes of DCo were estimated in the subtropical domains ($Co_{reg}/Co_{uptake} > 0.75$), consistent with the concept of oligotrophic areas being regenerated systems. At the high latitudes, the regeneration fluxes were low ($Co_{reg}/Co_{uptake} < 0.25$), with the lowest flux estimated in the SAG (10%). The equatorial area was marked by an intermediate regeneration rate, representing about 50% of the Co uptake flux. Hence, the regeneration can be the dominant internal source of DCo in the surface waters, especially in the subtropical domains.

The removal fluxes of Co by export via settling particles to deeper waters were 5 (in the NASG) to 25 (in the SAG) times lower than the biological uptake of DCo (Table 5), reinforcing the importance of surface recycling of biogenic Co in oligotrophic surface waters. Among the external sources to the surface waters, the inputs of DCo by the Amazon can be considered significant only in the northern equatorial area (>1 nmol m^{-2} d^{-1}), and to a lower extent in the southern side of the NASG. The atmospheric inputs of soluble Co were considered as significant in three areas, the SAW, the EA, and the NASG. However, the atmospheric source was relatively small compared to the other fluxes (Table 5), probably because low solubility of aerosols that can limit their impact.

Lateral advection by mesoscale structures can be an important term of the DCo budget at a local scale [*Dulaquais et al*., 2014]. These eddies can act either as intensive source or sink of DCo depending on whether they are cyclonic or anticyclonic [*Dulaquais et al*., 2014]. Nevertheless, the lateral input of DCo by these eddies would be negligible at the scale of a basin, such as in the subtropical domains (Table 5). By contrast, the advection of DCo-enriched surface waters like from the eastern Atlantic by the equatorial currents and from the Amazon plume entrained by the equatorial countercurrent, can represent a significant source of DCo at low latitudes (*Dulaquais et al*. [2014] and Table 5, respectively). Similarly, the lateral transport of DCo-enriched surface waters from high latitudes to DCo-depleted temperate waters by the Labrador Current in the North and by the Malvinas Current in the South can also represent important source terms in the DCo surface budgets (Table 5). At frontal systems, turbulence, and diffusivity could also account for a significant input of DCo from deep waters into the surface [*Dulaquais et al*., 2014] (Table 5).

The nearly conservative behavior of DCo observed at high latitudes in the north associated with the high DCo concentrations recorded in these surface waters are in line with the budget estimations that indicated strong inputs of DCo into the surface layer due to lateral advection of DCo-enriched waters from higher latitudes and comparatively low biological uptake (Table 5). It is possible that melting of Arctic ice enriched in DCo (e.g., $DCo_{ice}/DCo_{seawater} > 15$) [*Tovar-Sanchez et al*., 2010], as well as continental shelf enrichment along the surface waters circulation were significant sources of DCo at these high latitudes. Additionally, the estimated DCo uptake flux by phytoplankton increased southward from these high latitudes and this is in line with the observations that DCo showed a nearly conservative behavior that gradually changed to a nutrient-like vertical distribution in the southern side of the SAG (Figure 4a). It is conceivable that this seasonal biological removal of DCo would be partially resupplied by regeneration of DCo at the end of summer

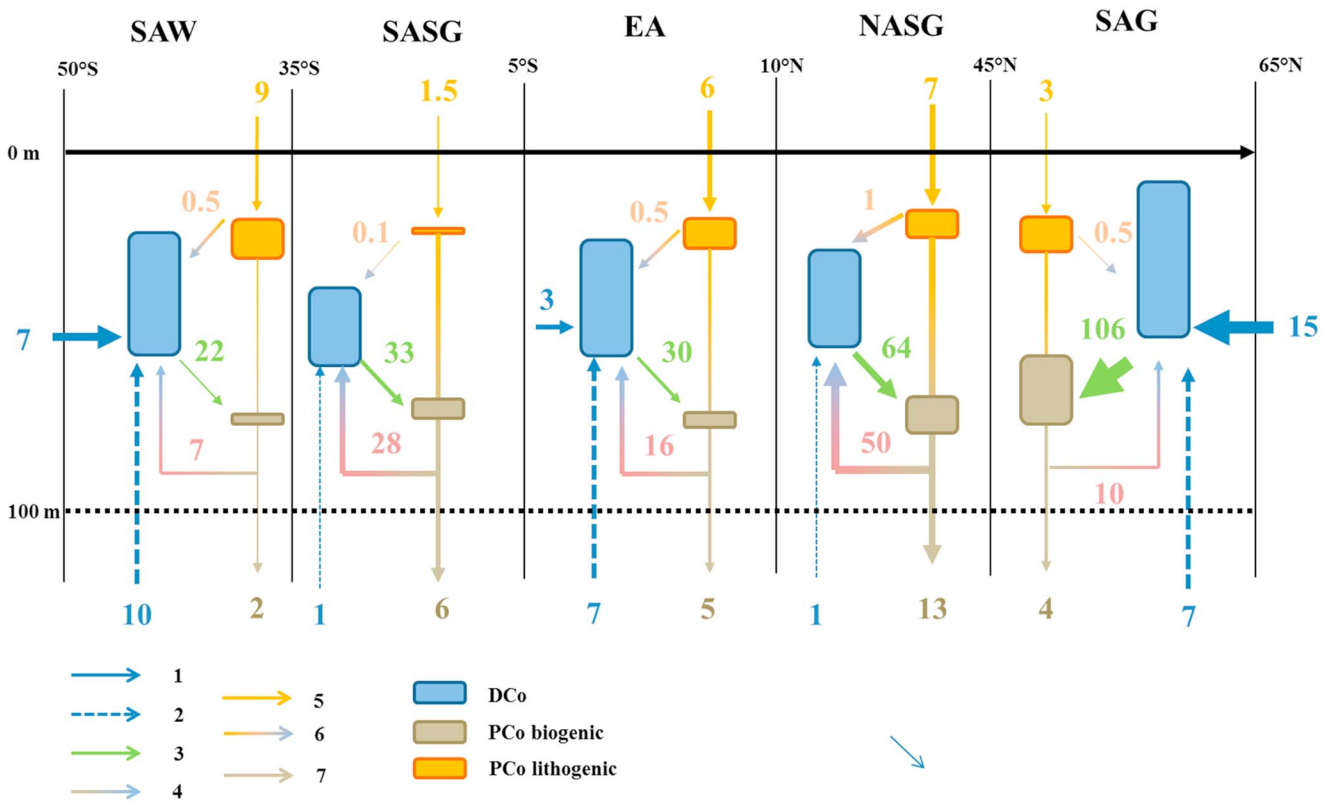

Figure 11. Conceptual schema of cobalt cycling in the different biogeochemical domains along the section. Wideness of the boxes represents the relative proportion of Co stock (at time of observation). Intensities of the fluxes are indicates and the numeration is described in Figure 7.

and by the mixing from wind-stress turbulence during late fall and winter times. In the subtropics, the nutrient-like P distributions of DCo (Figure 4a) fitted with the high biological uptake and extremely high regeneration rate (>80%) of DCo estimated for the oligotrophic gyres (Table 5). *Prochlorococcus* and *Synechococcus* sp. dominated the phytoplankton assemblage in those domains, and their high biological requirement for cobalt probably generated the surface DCo depletion. This nutrient-like distribution was recorded at different seasons [*Saito and Moffett*, 2002]; hence, it could be a permanent feature of the Co cycle in the oligotrophic systems. However, higher external inputs were detected in the northern gyre, especially due to the dust deposition during the dry season and to the Amazon River discharge during the wet season, and they generated an asymmetry between the two hemispheres (Figures 9b and 10 and Table 5). In the equatorial area, the physical processes can sustain the biological uptake of DCo both sides of the equator (Table 5). Relatively high vertical diffusion DCo fluxes due to the incursion of DCo-enriched Atlantic Central Waters [*Dulaquais et al*., 2014] may indeed constitute a substantial source of DCo there (Table 5), in addition to the westward lateral advection of DCo-enriched waters by the equatorial currents system [*Dulaquais et al*., 2014]. The inputs by the physical dynamics can actually sustain up to 40% of the DCo drawdown due to biological uptake on both sides of the equator.

The global budget (DCo + PCo) at the scale of the western Atlantic (Table 5) clearly showed that the subtropical domains are acting as sink of Co (approximately −1100 t of Co/year), especially in the NASG. In contrast, high latitudes and equatorial Atlantic constituted sources of Co into the surface western Atlantic, balancing the sink determined in the subtropics (approximately +1200 t of Co/year). This mass balance suggests exchanges between the different domains probably through circulation of intermediate waters and transport by eddies. The MBC and the equatorial current system indeed supply eddies to the south and north subtropics, respectively. These dynamic structures can then supply in DCo the subtropics by advection of enriched surface waters, as well as by vertical advection/diffusion of DCo from intermediate waters wherein concentrations are higher. Like dust events, blooms, and export flux, eddy events can vary

seasonally. Thus, the seasonal variability within the different domains must be taken into account to understand the biogeochemical cycle of cobalt in the surface western Atlantic.

5. Conclusions

Significant regional correlations were observed between DCo and P across the different biological domains of the western Atlantic Ocean in part due to differences in the phytoplankton community composition. For instance, the highest DCo:P depletion ratios recorded in the two subtropical domains were related to an absolute requirement for DCo of the dominant cyanobacteria species, whereas the low DCo:P recorded in the subantarctic waters could reflect the low Co requirement of diatoms.

Biological uptake was the main sink of DCo in the surface waters of the western Atlantic, resulting in the overall nutrient-like distribution of DCo. The covariation of biogenic PCo and Chl *a* further supports the micronutritive behavior of Co. The higher biological assimilation rates of DCo by cyanobacteria at tropical latitudes compared to subpolar and subantarctic domains, can lead to the decreasing gradients of surface DCo observed from the high to the low latitudes along the western Atlantic. Regeneration that includes abiotic processes, microbial loop, cell lysis, and grazing was the prevailing internal source of DCo in oligotrophic surface waters, sustaining up to 85% of the biological DCo drawdown. Overall, the internal cycle of DCo was primarily driven by the two processes of biological uptake and regeneration.

The atmospheric input was a significant source of DCo to the Northern Hemisphere and generated an asymmetry in DCo concentrations between the north and south subtropical domains. The Amazon River accounted for up to 50% of the DCo inventory of the mixed layer in the tropical northwestern Atlantic, but its impact rapidly decreased away from the mouth. Together, these external sources can sustain the higher biological demand of DCo estimated in the northern subtropical gyre compared to the southern gyre.

Advection of DCo-enriched waters from the high latitudes can be source of DCo especially to the subpolar Atlantic, a region characterized by a low Co regeneration rate. Moreover, lateral advection and vertical diffusion can sustain the biological demand of DCo in the equatorial area.

Constraining the different sources and sinks has also allowed estimation of the DCo residence time in the upper 100 m. Short residence times driven by physical processes were determined at high northern latitudes (~0.7 year), whereas residence times were more than 2 times longer in the regenerated systems of the subtropics (~1.5 years).

Tentative budgets of Co in surface waters were assessed and they suggested nonsteady state regimes at the scale of each biogeochemical domain. At the scale of the western Atlantic basin, the loss of Co (dissolved plus particulate) in the subtropics could be balanced by the gain at the high latitudes and in the equatorial area. Exchanges and transportation from source regions (high latitudes) to sink regions (subtropics) through dynamic features (surface jets, eddies, and circulation at intermediate depths) could balance the Co budget in the western Atlantic basin.

This study has demonstrated the importance of variability in internal cycling and external sources of DCo across biogeochemical domains to regional and basin-scale Co budgets. This work also provides new keys to the parameterization of cobalt biogeochemistry in marine systems, which can be implemented in future three-dimensional global models of the oceanic cobalt cycle.

Acknowledgments

The complete data set of cobalt (dissolved, total, and apparent particulate) at all stations is available at the international GEOTRACES datacenter (http://www.bodc.ac.uk/geotraces/). We are indebted to the Captains, officers, and crew members of the R.V. *Pelagia* and R.S.S. *James Cook*: without their exceptional support, this large ocean section would not have been possible. We are most grateful to Loes Gerringa and Micha Rijkenberg, the chief scientists of the cruises. We warmly thank Jan van Ooijen, K. Bakker, E. van Weerlee, and S. Ossebaar for the analyses of nutrients, as well as S. Ober, Martin Laan, Steven van Heuven, S. Asjes, and L. Wuis for providing high-quality CTD data. We are much grateful to M. Rutgers van der Loeff for providing the particulate carbon data in the west northern Atlantic, R. Shelley for communication on cobalt concentrations in North Atlantic aerosols, and P.J. Lam for communication on cobalt/carbon ratio in the different size class of west northern Atlantic marine particles. This investigation was supported by the GEOTRACES-GEOSECS revisited in the West Atlantic project coordinated by M. Boye and funded by the French LEFE-CYBER National Program of the Institut National des Sciences de l'Univers (INSU). We also acknowledge the European COST-Action ES801 for funding a short-term Scientific Mission to G. Dulaquais to join the last cruise of the GEOTRACES-A02 section. The Université de Bretagne Occidentale (UBO) and the Région Bretagne (ARED) are supporting the PhD fellowship of G. Dulaquais. P.M. was supported in part by a Gledden Visiting Fellowship awarded by the Institute of Advanced Studies at The University of Western Australia. This investigation is a contribution to the international GEOTRACES program. We warmly thank the two referees Mak Saito and Johann Bown for their comments and constructive remarks.

References

Arrigo, K. R., D. Worthen, A. Schnell, and M. P. Lizotte (1998), Primary production in Southern Ocean waters, *J. Geophys. Res.*, *103*(C8), 15,587–15,600, doi:10.1029/98JC00930.

Aucour, A. M., F. X. Tao, P. Moreira-Turcq, P. Seyler, S. Sheppard, and M. F. Benedetti (2003), The Amazon River: Behaviour of metals (Fe, Al, Mn) and dissolved organic matter in the initial mixing at the Rio Negro/Solimoes confluence, *Chem. Geol.*, *197*(1), 271–285.

Baker, A. R., K. Weston, S. D. Kelly, M. Voss, P. Streu, and J. N. Cape (2007), Dry and wet deposition of nutrients from the tropical Atlantic atmosphere: Links to primary productivity and nitrogen fixation, *Deep Sea Res., Part I*, *54*, 1704–1720.

Baker, A. R., C. Adams, T. G. Bell, T. D. Jickells, and L. Ganzeveld (2013), Estimation of atmospheric nutrient inputs to the Atlantic Ocean from 50°N to 50°S based on large-scale field sampling: Iron and other dust-associated elements, *Global Biogeochem. Cycles*, *27*, 755–767, doi:10.1002/gbc.20062.

Bertilsson, S., O. Berglund, D. M. Karl, and S. W. Chisholm (2003), Elemental composition of marine *Prochlorococcus* and *Synechococcus*: Implications for the ecological stoichiometry of the sea, *Limnol. Oceanogr.*, *48*, 1721–1731.

Bertrand, E. M., M. A. Saito, J. M. Rose, C. R. Riesselman, M. C. Lohan, A. E. Noble, P. A. Lee, and G. R. DiTullio (2007), Vitamin B12 and iron co-limitation of phytoplankton growth in the Ross Sea, *Limnol. Oceanogr.*, *52*, 1079–1093.
Bonnet, S., E. A. Webb, C. Panzeca, D. M. Karl, D. G. Capone, and S. A. Sañudo-Wilhelmy (2010), Vitamin B12 excretion by cultures of the marine cyanobacteria Crocosphaera and Synechococcus, *Limnol. Oceanogr.*, *55*(5), 1959–1964.
Bowie, A. R., and M. C. Lohan (2009), Analysis of iron in seawater, in *Practical Guidelines for the Analysis of Seawater*, chap. 12, edited by O. Wurl, pp. 235–257, Taylor and Francis, Boca Raton, Fla.
Bown, J., M. Boye, A. Baker, E. Duvieilbourg, F. Lacan, F. Le Moigne, F. Planchon, S. Speich, and D. M. Nelson (2011), The biogeochemical cycle of dissolved cobalt in the Atlantic and the Southern Ocean south off the coast of South Africa, *Mar. Chem.*, *126*, 193–206, doi:10.1016/j.marchem.2011.03.008.
Bown, J., M. Boye, and D. M. Nelson (2012), New insights on the role of organic speciation in the biogeochemical cycle of dissolved cobalt in the southeastern Atlantic and the Southern Ocean, *Biogeosciences*, *9*, 2719–2736.
Boyle, E. A., S. S. Huested, and B. Grant (1982), The chemical mass balance of the Amazon Plume II. Copper, nickel, and cadmium, *Deep Sea Res., Part A.*, *29*(11), 1355–1364.
Brown, C. W., and J. A. Yoder (1994), Coccolithophorid blooms in the global ocean, *J. Geophys. Res.*, *99*(C4), 7467–7482, doi:10.1029/93JC02156.
Browning, T. J., H. A. Bouman, C. M. Moore, C. Schlosser, G. A. Tarran, E. M. S. Woodward, and G. M. Henderson (2014), Nutrient regimes control phytoplankton ecophysiology in the South Atlantic, *Biogeosciences*, *11*(2), 463–479.
Bruland, K. W., and R. P. Franks (1983), Mn, Ni, Cu, Zn and Cd in the western North Atlantic, in *Trace Metals in Sea Water*, edited by C. S. Wong et al., pp. 395–414, Springer, New York.
Campbell, L., H. A. Nolla, and D. Vaulot (1994), The importance of Prochlorococcus to community structure in the central North Pacific Ocean, *Limnol. Oceanogr.*, *39*, 954–961, doi:10.4319/lo.1994.39.4.0954.
Church, T. M. (1986), Biogeochemical factors influencing the residence time of microconstituents in a large tidal estuary, Delaware Bay, *Mar. Chem.*, *18*(2), 393–406.
Croot, P. L., O. Baars, and P. Streu (2011), The distribution of dissolved zinc in the Atlantic sector of the Southern Ocean, *Deep Sea Res., Part II*, *58*(25), 2707–2719.
Cullen, J. T., Z. Chase, K. H. Coale, S. E. Fitzwater, and R. M. Sherrell (2003), Effect of iron limitation on the cadmium to phosphorus ratio of natural phytoplankton assemblages from the Southern Ocean, *Limnol. Oceanogr.*, *48*, 1079–1087.
Dammshäuser, A., T. Wagener, and P. L. Croot (2011), Surface water dissolved aluminum and titanium: Tracers for specific time scales of dust deposition to the Atlantic?, *Geophys. Res. Lett.*, *38*, L24601, doi:10.1029/2011GL049847.
de Baar, H. J. W., et al. (2008), Titan: A new facility for ultraclean sampling of trace elements and isotopes in the deep oceans in the international GEOTRACES program, *Mar. Chem.*, *111*(1–2), 4–21.
de Jong, J. T. M., M. Boye, M. D. Gelado-Caballero, K. R. Timmermans, M. J. W. Veldhuis, R. F. Nolting, C. M. G. van den Berg, and H. J. W. de Baar (2007), Inputs of iron, manganese and aluminium to surface waters of the Northeast Atlantic Ocean and the European continental shelf, *Mar. Chem.*, *107*, 120–142.
Dulaquais, G., M. Boye, M. J. A. Rijkenberg, and X. Carton (2014), Physical and remineralization processes govern the cobalt distribution in the deep western Atlantic Ocean, *Biogeosciences*, *11*(6), 1561–1580.
Ellwood, M. J. (2008), Wintertime trace metal (Zn, Cu, Ni, Cd, Pb and Co) and nutrient distributions in the subantarctic zone between 40–52 S; 155–160 E, *Mar. Chem.*, *112*(1), 107–117.
Ferreira, A., D. Stramski, C. A. Garcia, V. M. Garcia, A. M. Ciotti, and C. R. Mendes (2013), Variability in light absorption and scattering of phytoplankton in Patagonian waters: Role of community size structure and pigment composition, *J. Geophys. Res. Oceans*, *118*, 698–714, doi:10.1002/jgrc.20082.
Field, C. B., M. J. Behrenfeld, J. T. Randerson, and P. Falkowski (1998), Primary production of the biosphere: Integrating terrestrial and oceanic components, *Science*, *281*(5374), 237–240.
Flatau, M. K., L. Talley, and P. P. Niiler (2003), The North Atlantic Oscillation, surface current velocities, and SST changes in the subpolar North Atlantic, *J. Clim.*, *16*(14), 2355–2369.
Gaiero, D. M., J.-L. Probst, P. J. Depetris, S. M. Bidart, and L. Leleyter (2003), Iron and other transition metals in Patagonian riverborne and windborne materials: Geochemical control and transport to the southern South Atlantic Ocean, *Geochim. Cosmochim. Acta*, *67*(19), 3603–3623.
Ginoux, P., M. Chin, I. Tegen, J. M. Prospero, B. Holben, O. Dubovik, and S. J. Lin (2001), Sources and distributions of dust aerosols simulated with the GOCART model, *J. Geophys. Res.*, *106*(D17), 20,255–20,273, doi:10.1029/2000JD000053.
Goldman, J. C. (1988), Spatial and temporal discontinuities of biological processes in pelagic surface waters, in *Toward a Theory on Biological-Physical Interactions in the World Ocean*, edited by B. J. Rothschild, pp. 273–296, Kluwer Acad., Dordrecht, Netherlands.
Goldman, J. C. (1993), Potential role of large oceanic diatoms in new primary production, *Deep Sea Res., Part I*, *40*, 159–168.
Gong, N., C. Chen, X. Liping, H. Chen, X. Lin, and R. Zhang (2005), Characterization of a thermostable alkaline phosphatase from a novel species Thermus yunnanensis sp. nov. and investigation of its cobalt activation at high temperature, *Biochim. Biophys. Acta, Proteins Proteomics*, *1750*, 103–111.
Grasshoff, K., M. Ehrhardt, and K. Kremling (1983), *Methods of Seawater Analysis*, pp. 419, Verlag Chemie GmbH, Weinheim, Germany.
Gregg, W. W., and N. W. Casey (2007), Modeling coccolithophores in the global oceans, *Deep Sea Res., Part II*, *54*, 447–477.
Head, E. J. H., L. R. Harris, and R. W. Campbell (2000), Investigations on the ecology of Calanus spp. in the Labrador Sea. I. Relationship between the phytoplankton bloom and reproduction and development of Calanus finmarchicus in spring, *Mar. Ecol. Prog. Ser.*, *193*, 53–73.
Hellweger, F. L., and A. L. Gordon (2002), Tracing Amazon River water into the Caribbean Sea, *J. Mar. Res.*, *60*, 537–549.
Ho, T. Y., A. Quigg, Z. V. Finkel, A. J. Milligan, K. Wyman, P. G. Falkowski, and F. M. M. Morel (2003), The elemental composition of some marine phytoplankton, *J. Phycol.*, *39*(6), 1145–1159.
Jakuba, R. W., J. W. Moffett, and S. T. Dyhrman (2008), Evidence for the linked biogeochemical cycling of zinc, cobalt, and phosphorus in the western North Atlantic Ocean, *Global Biogeochem. Cycles*, *22*, GB4012, doi:10.1029/2007GB003119.
Jenkins, W. J., and J. C. Goldman (1985), Seasonal oxygen cycling and primary production in the Sargasso Sea, *J. Mar. Res.*, *43*(2), 465–491.
Ji, Y., and R. M. Sherrell (2008), Differential effects of phosphorus limitation on cellular metals in Chlorella and Microcystis, *Limnol. Oceanogr.*, *53*, 1790–1804.
Jickells, T. S., et al. (2005), Global iron connections between desert dust, ocean biogeochemistry and climate, *Science*, *308*, 67–71.
Lane, T. W., and F. M. M. Morel (2000), Regulation of carbonic anhydrase expression by zinc, cobalt, and carbon dioxide in the marine diatom *Thalassiosira weissflogii*, *Plant Physiol.*, *123*, 345–352, doi:10.1104/pp.123.1.345.

Lomas, M. W., and S. B. Moran (2011), Evidence for aggregation and export of cyanobacteria and nano-eukaryotes from the Sargasso Sea euphotic zone, *Biogeosciences*, *8*(1), 203–216, doi:10.5194/bg-8-203-2011.
Mahowald, N. M., A. R. Baker, G. Bergametti, N. Brooks, R. A. Duce, T. D. Jickells, N. Kubilay, J. M. Prospero, and I. Tegen (2005), Atmospheric global dust cycle and iron inputs to the ocean, *Global Biogeochem. Cycles*, *19*, GB4025, doi:10.1029/2004GB002402.
Mann, E. L. (2000), Trace metals and the ecology of marine cyanobacteria, PhD thesis, MIT/WHOI Joint Program in Oceanography, Cambridge, Mass.
Martin, J. H., S. E. Fitzwater, R. M. Gordon, C. N. Hunter, and S. J. Tanner (1993), Iron, primary production and carbon nitrogen flux studies during the JGOFS North-Atlantic bloom experiment, *Deep Sea Res., Part I*, *40*(1–2), 115–134.
Mather, R., S. Reynolds, G. Wolff, R. G. Williams, S. Torres-Valdes, E. M. S. Woodward, A. Landolfi, X. Pan, R. W. Sanders, and E. Achterberg (2008), Phosphorus cycling in the North and South Atlantic Ocean subtropical gyres, *Nat. Geosci.*, *1*, 439–443.
McLaughlin, K., J. A. Sohm, G. A. Cutter, M. W. Lomas, and A. Paytan (2013), Phosphorus cycling in the Sargasso Sea: Investigation using the oxygen isotopic composition of phosphate, enzyme-labeled fluorescence, and turnover times, *Global Biogeochem. Cycles*, *27*, 375–387, doi:10.1002/gbc.20037.
Measures, C. I., and E. T. Brown (1996), Estimating dust input to the Atlantic Ocean using surface water Al concentrations, in *The Impact of African Dust Across the Mediterranean*, edited by S. Guerzoni and R. Chester, pp. 389, Kluwer Acad., Dordrecht, Netherlands.
Measures, C. I., and S. Vink (2000), On the use of dissolved aluminium in surface waters to estimate dust deposition to the ocean, *Global Biogeochem. Cycles*, *14*, 317–327, doi:10.1029/1999GB001188.
Middag, R., H. J. W. de Baar, P. Laan, and K. Bakker (2009), Dissolved aluminium and the silicon cycle in the Arctic Ocean, *Mar. Chem.*, *115*, 176–195, doi:10.1016/j.marchem.2009.08.002.
Minobe, S., M. Miyashita, A. Kuwano-Yoshida, H. Tokinaga, and S. P. Xie (2010), Atmospheric response to the gulf stream: Seasonal variations, *J. Clim.*, *23*(13), 3699–3719, doi:10.1175/2010JCLI3359.1.
Moffett, J. W., and J. Ho (1996), Oxidation of cobalt and manganese in seawater via a common microbially catalyzed pathway, *Geochim. Cosmochim. Acta*, *60*(18), 3415–3424.
Molleri, G. S. F., E. M. L. de M. Novo, and M. Kampel (2010), Space-time variability of the Amazon River plume based on satellite ocean color, *Cont. Shelf Res.*, *30*, 342–352.
Moore, W. S., J. L. Sarmiento, and R. M. Key (1986), Tracing the Amazon component of surface Atlantic water using 228Ra, salinity and silica, *J. Geophys. Res.*, *91*(C2), 2574–2580, doi:10.1029/JC091iC02p02574.
Moran, S. B., and R. M. Moore (1988), Evidence from mesocosm studies for biological removal of dissolved aluminum from sea water, *Nature*, *335*, 706–708, doi:10.1038/335706a0.
Murphy, J., and J. P. Riley (1962), A modified single solution method for the determination of phosphate in natural waters, *Anal. Chim. Acta*, *27*, 31–36.
Noble, A. E., M. A. Saito, K. Maiti, and C. R. Benitez-Nelson (2008), Cobalt, manganese, and iron near the Hawaiian Islands: A potential concentrating mechanism for cobalt within a cyclonic eddy and implications for the hybrid-type trace metals, *Deep Sea Res., Part II*, *55*, 1473–1490, doi:10.1016/j.dsr2.2008.02.010.
Noble, A. E., et al. (2012), Basin scale inputs of cobalt, iron, and manganese from the Benguela-Angola front to the South Atlantic Ocean, *Limnol. Oceanogr.*, *57*, 989–1010.
Okada, H., and A. McIntyre (1979), Seasonal distribution of modern coccolithophores in the western North Atlantic Ocean, *Mar. Biol.*, *54*, 319–328.
Oschlies, A., and V. Garçon (1998), Eddy-induced enhancement of primary production in a model of the North Atlantic Ocean, *Nature*, *394*, 266–269.
Owens, S. A., Pike, S., and K. O. Buesseler (2014), Thorium-234 as a tracer of particle dynamics and upper ocean export in the Atlantic Ocean, *Deep Sea Res., Part II*, in press.
Panzeca, C., A. J. Beck, K. Leblanc, G. T. Taylor, D. A. Hutchins, and S. A. Sañudo-Wilhelmy (2008), Potential cobalt limitation of vitamin B12 synthesis in the North Atlantic Ocean, *Global Biogeochem. Cycles*, *22*, GB2029, doi:10.1029/2007GB003124.
Parsons, T. R., and C. M. Lalli (1988), Comparative oceanic ecology of the plankton communities of the subarctic Atlantic and Pacific Oceans, *Oceanogr. Mar. Biol., Annu. Rev.*, *26*, 317–359.
Peterson, R. G., and L. Stramma (1991), Upper-level circulation in the South Atlantic Ocean, *Prog. Oceanogr.*, *26*, 1–73, doi:10.1016/0079-6611(91)90006-8.
Peterson, R. G., C. S. Johnson, W. Krauss, and R. E. Davis (1996), Lagrangian measurements in the Malvinas Current, in *The South Atlantic. Present and Past Circulation*, edited by G. Wefer et al., pp. 239–247, Springer, New York.
Prospero, J. M., and P. J. Lamb (2003), African droughts and dust transport to the Caribbean: Climate change implications, *Science*, *302*, 1024–1027.
Reid, J. L. (1994), On the total geostrophic circulation of the North Atlantic Ocean: Flow patterns, tracers and transports, *Prog. Oceanogr.*, *33*, 1–92.
Reid, E. A., J. S. Reid, M. M. Meier, M. R. Dunlap, S. S. Cliff, A. Broumas, K. Perry, and H. Maring (2003), Characterization of African dust transported to Puerto Rico by individual particle and size segregated bulk analysis, *J. Geophys. Res.*, *108*(D19), 8591, doi:10.1029/2002JD002935.
Rijkenberg, M. J., R. Middag, P. Laan, L. J. Gerringa, H. M. van Aken, V. Schoemann, J. T. M. de Jong, and H. J. de Baar (2014), The distribution of dissolved iron in the West Atlantic Ocean, *PLoS One*, *9*(6), e101323, doi:10.1371/journal.pone.0101323.
Rudnick, R. L., and S. Gao (2003), Composition of the continental crust, in *The Crust*, edited by R. L. Rudnick, pp. 1–70, Elsevier, Amsterdam.
Saito, M. A., and J. W. Moffett (2001), Complexation of cobalt by natural organic ligands in the Sargasso Sea as determined by a new high sensitivity electrochemical cobalt speciation method suitable for open ocean work, *Mar. Chem.*, *75*, 49–68.
Saito, M. A., and J. W. Moffett (2002), Temporal and spatial variability of cobalt in the Atlantic Ocean, *Geochim. Cosmochim. Acta*, *66*, 1943–1953.
Saito, M. A., J. W. Moppett, S. W. Chisholm, and J. B. Waterbury (2002), Cobalt limitation and uptake in Prochlorococcus, *Limnol. Oceanogr.*, *47*(6), 1629–1636.
Saito, M. A., J. W. Moffett, and G. R. DiTullio (2004), Cobalt and nickel in the Peru upwelling region: A major flux of labile cobalt utilized as a micronutrient, *Global Biogeochem. Cycles*, *18*, GB4030, doi:10.1029/2003GB002216.
Saito, M. A., G. Rocap, and J. W. Moffett (2005), Production of cobalt binding ligands in a Synechococcus feature at the Costa Rica Upwelling Dome, *Limnol. Oceanogr.*, *50*, 279–290, doi:10.4319/lo.2005.50.1.0279.
Saito, M. A., T. J. Goepfert, A. E. Noble, E. M. Bertrand, P. N. Sedwick, and G. R. DiTullio (2010), A seasonal study of dissolved cobalt in the Ross Sea, Antarctica: Micronutrient behavior, absence of scavenging, and relationships with Zn, Cd, and P, *Biogeosciences*, *7*, 4059–4082, doi:10.5194/bg-7-4059-2010.
Seyler, P., and G. R. Boaventura (2003), Trace elements in the mainstream Amazon River, in *The Biochemistry of the Amazon Basin*, edited by M. E. McClain, pp. 534, Oxford Univ. Press, Oxford, U. K.

Shelley, R. U., B. Zachhuber, P. N. Sedwick, P. J. Worsfold, and M. C. Lohan (2010), Determination of total dissolved cobalt in UV-irradiated seawater using flow injection with chemiluminescence detection, *Limnol. Oceanogr.*, *8*, 352–362, doi:10.4319/lom.2010.8.352.

Shelley, R. U., et al. (2012), Controls on dissolved cobalt in surface waters of the Sargasso Sea: Comparisons with iron and aluminum, *Global Biogeochem. Cycles*, *26*, GB2020, doi:10.1029/2011GB004155.

Sherrell, R. M., and E. A. Boyle (1992), The trace metal composition of suspended particles in the oceanic water column near Bermuda, *Earth Planet. Sci. Lett.*, *111*, 155–174.

Silver, M. W., M. M. Gowing, and P. J. Davoll (1986), The association of photosynthetic picoplankton and ultraplankton with pelagic detritus through the water column (0–2000 m), *Can. Bull. Fish. Aquat. Sci.*, *214*, 311–341.

Smoak, J. M., J. M. Krest, and P. W. Swarzenski (2006), Geochemistry of the Amazon estuary, in *Estuaries*, pp. 71–90, Springer, Berlin Heidelberg.

Stramma, L., and M. England (1999), On the water masses and mean circulation of the South Atlantic Ocean, *J. Geophys. Res.*, *104*(C9), 20,863–20,883, doi:10.1029/1999JC900139.

Strickland, J. D. H., and T. R. Parsons (1968), A practical handbook of seawater analysis. First Edition, Fisheries Research Board of Canada, Bulletin. No 167, p.65.

Subramaniam, A., et al. (2008), Amazon River enhances diazotrophy and carbon sequestration in the tropical North Atlantic Ocean, *Proc. Natl. Acad. Sci. U.S.A.*, *105*(30), 10,460–10,465.

Sunda, W. G., and S. A. Huntsman (1995), Cobalt and zinc inter-replacement in marine phytoplankton: Biological and geochemical implications, *Limnol. Oceanogr.*, *40*, 1404–1417.

Swanner, E. D., N. J. Planavsky, S. V. Lalonde, L. J. Robbins, A. Bekker, O. J. Rouxel, M. A. Saito, A. Kappler, S. J. Mojzsis, and K. O. Konhauser (2014), Cobalt and marine redox evolution, *Earth Planet. Sci. Lett.*, *390*, 253–263.

Takahashi, M., and P. K. Bienfang (1983), Size-structure of phytoplankton biomass and photosynthesis in subtropical Hawaiian waters, *Mar. Biol.*, *76*, 203–211.

Tang, D., and F. F. M. Morel (2006), Distinguishing between cellular and Fe-oxide-associated trace elements in phytoplankton, *Mar. Chem.*, *98*(1), 18–30.

Tegen, I., M. Werner, S. P. Harrison, and K. E. Kohfeld (2004), Relative importance of climate and land use in determining present and future global soil dust emission, *Geophys. Res. Lett.*, *31*, L05105, doi:10.1029/2003GL019216.

Tomczak, M., and J. S. Godfrey (2003), *Regional Oceanography: An Introduction*, 2nd ed., pp. 422, Pergamon, Oxford, U. K.

Tovar-Sanchez, A., and S. A. Sañudo-Wilhelmy (2011), Influence of the Amazon River on dissolved and intra-cellular metal concentrations in *Trichodesmium* colonies along the western boundary of the sub-tropical North Atlantic Ocean, *Biogeosciences*, *8*, 217–225, doi:10.5194/bg-8-217-2011.

Tovar-Sanchez, A., S. A. Sañudo-Wilhelmy, A. B. Kustka, S. Agusti, J. Dachs, D. A. Hutchins, D. G. Capone, and C. M. Duarte (2006), Effects of dust deposition and river discharges on trace metal composition of *Trichodesmium spp.* in the tropical and subtropical North Atlantic Ocean, *Limnol. Oceanogr.*, *51*(4), 1755–1761.

Tovar-Sanchez, A., C. M. Duarte, J. C. Alonso, S. Lacorte, R. Tauler, and C. Galban-Malagon (2010), Impacts of metals and nutrients released from melting multiyear Arctic sea ice, *J. Geophys. Res.*, *115*, C07003, doi:10.1029/2009JC005685.

Trapp, J. M., F. J. Millero, and J. M. Prospero (2010), Temporal variability of the elemental composition of African dust measured in trade wind aerosols at Barbados and Miami, *Mar. Chem.*, *120*(1–4), 71–82, doi:10.1016/j.marchem.2008.10.004.

Twining, B. S., and S. B. Baines (2013), The trace metal composition of marine phytoplankton, *Annu. Rev. Mar. Sci.*, *5*, 191–215.

Twining, B. S., S. B. Baines, J. B. Bozard, S. Vogt, E. A. Walker, and D. M. Nelson (2011), Metal quotas of plankton in the equatorial Pacific Ocean, *Deep Sea Res., Part II*, *58*(3), 325–341.

van Hulten, M. M. P., A. Sterl, A. Tagliabue, J. C. Dutay, M. Gehlen, H. J. De Baar, and R. Middag (2013), Aluminium in an ocean general circulation model compared with the West Atlantic Geotraces cruises, *J. Mar. Syst.*, *126*, 3–23.

van Ooijen, J. (2010), Nutrient measurements, Cruise Report 64PE319, 17-19.

Vink, S., and C. I. Measures (2001), The role of dust deposition in determining surface water distributions of Al and Fe in the South West Atlantic, *Deep Sea Res., Part II*, *48*(13), 2787–2809.

Weinstein, S. E., and S. B. Moran (2004), Distribution of size-fractionated particulate trace metals collected by bottles and in-situ pumps in the Gulf of Maine–Scotian Shelf and Labrador Sea, *Mar. Chem.*, *87*(3), 121–135.

Xia, L., and Y. Gao (2010), Chemical composition and size distributions of coastal aerosols observed on the US East Coast, *Mar. Chem.*, *119*(1), 77–90.